Introduction

by D. Quéré and C. Clanet

Science is a language, and as such, a way to watch at things and to share ideas. And it is always fascinating to realize how a particular facet of truth emerges from the translation of things in a given language, and conversely how the multiplicity of languages, or points of view, allows us to approach and to define this thing. Poetry, physics, painting, all have something to say of a tree or of a stone, and we need all of them. This implies that it is always fruitful, and even surprising, to turn the science's gaze on something on which we are not used to have this kind of gaze. We propose in this book to observe sports with the eyes of science, trying to express physical laws, to connect disconnected facts, to classify, and even, ideally, to generate news ideas and original questions beyond the field of observation – a sport field here.

We occasionally meet sport in the historical scientific literature, often used to illustrate a physical principle or law [1]. One of the most striking example in this spirit can be found in Descartes, where the trajectory of light is compared to the one of balls in real tennis, or jeu de paume [2]: *Ce que ceux qui jouent à la paume éprouvent assez, lorsque leur balle rencontre de faux carreaux, ou bien qu'ils la touchent en biaisant de leur raquette, ce qu'ils nomment, ce me semble, couper ou friser.* This analogy was developed by Newton in 1671, when he published his New Theory about Light and Colors in the Philosophical Transactions [3]: *Then I began to suspect, whether the Rays, after their trajection through the Prisme, did not move in curve lines. And it increased my suspicion when I remembred that I had often seen a Tennis ball, struck with an oblique Racket, describe a curve line.* Apart from the unexpected use of the word "tennis" more than one century before its official creation in England, we can suspect that the analogy with sport was also used by Newton to convince his readers, who had probably spent more time playing games than observing light.

These curved lines in tennis continued to excite the curiosity of English scientists, since Lord Rayleigh discussed them two centuries later, in the Messenger of Mathematics in 1877 [4]. There he applied Magnus theory to account for the special aerodynamics of spinning spheres, an excellent example of the ability of sports to generate original questions of much broader impact. We do not wish to be exhaustive in this short introduction. But covering the links between Science and Sport with seven-league boots, we would like to cite here the wonderful 1974 paper by Jo Keller

about the best way to run a race, and tackled using variational approach [5,6]; or the work by Brooke Benjamin and his student Charles Reep in 1968 inspired by methods in statistical physics to understand the number of passes in soccer before losing the ball [7].

Indeed, these papers are perfect examples of what we would like to do in this book, which is a collective work following a conference on the Physics of Sports organized at Ecole Polytechnique in April 2012. During the Olympic Games of the same year, Pierre Lepidi and David Larrousserie from the journal Le Monde published a series of short papers on sport seen from a scientific viewpoint, and they kindly accepted to collect these papers in the first chapter of this book. We then share the different topics covered by the conference in six parts, which out of this context could be the titles of textbooks in Physics or Fluid Mechanics, namely: Waves and Fluids, Aerodynamics, Elasticity, Friction, Statistical Physics, and Human Motion. We hope that our readers will find along these chapters a reflection of our common enthusiasm in exploring the often-virgin territory of Sports Physics !

References

[1] Frohlich, C., 2011, Resource letter PS-2: Physics of sports In *Amer. J. Physics*, **79**, pp. 565-574.

[2] Descartes R., 1637, La Dioptrique In *Oeuvres de René Descartes*.

[3] Newton, I., 1671, New Theory about Light and Colors In *Philosophical Transactions*, **6**, pp. 3075-3087.

[4] Rayleigh, L., 1877, On the irregular flight of a tennis ball In *Messenger of Mathematics*, **7**, pp. 14-16.

[5] Keller, J.B., 1973, A theory of competitive running In *Physics Today*, **26**, pp. 42-47.

[6] Keller, J.B., 1974, Optimal velocity in a race In *American Mathematical Monthly*, **81**, pp. 474-480.

[7] Reep C. and B. Benjamin, 1968, Skill and Chance in Association Football In *Journal of the Royal Statistical Society. Series A* **131**, pp. 581-585.

2 The aerodynamics of the beautiful game

by J.W.M. Bush
Department of Mathematics, MIT

Abstract

We consider the aerodynamics of football, specifically, the interaction between a ball in flight and the ambient air. Doing so allows one to account for the characteristic range and trajectories of balls in flight, as well as their anomalous deflections as may be induced by striking the ball either with or without spin. The dynamics of viscous boundary layers is briefly reviewed, its critical importance on the ball trajectories highlighted. The Magnus effect responsible for the anomalous curvature of spinning balls is seen to depend critically on the surface roughness of the ball, the sign of the Magnus force reversing for smooth balls. The origins of the fluttering of balls struck with nearly no spin is also discussed. Particular attention is given to categorizing and providing aerodynamic rationale for the various free kick styles.

1 Introduction

Fluid dynamics is the science that allows us to rationalize the flow of fluids, either liquids or gases, and so understand a vast array of everyday phenomena (Batchelor 1967, Acheson 1990). Aerodynamics is the subset of fluid dynamics dealing with the flow of air. In addition to informing the design of airplanes and providing the rationale for the flight of birds and insects, it provides the basis for understanding the trajectory of sports balls in flight. A comprehensive treatment of this more general subject, sports ball aerodynamics, can be found in Daish (1972), Mehta (1985, 2009) and Mehta & Pallis (2001), while the aerodynamics of specific sports, including golf (Erlichson 1983), cricket (Mehta *et al.* 1983, Mehta 2005), tennis (Mehta *et al.* 2008), baseball (Watts & Sawyer 1975, Frolich 1984, Adair 2002, Nathan 2008) and american football (Gay 2004) have been treated elsewhere. We here focus specifically on the dynamics of soccer, or as most of the world knows it, football. The bulk of the research reported here is not original. While it does draw in part upon recent studies of the aerodynamics of football (Asai *et al.* 2007, Hong *et al.* 2010, Dupeux *et al.* 2010, Hong & Asai 2011, Goff 2010, Goff & Carré 2010, 2012), it is more a personal than a scholarly account, an idiosynchratic pedagogical review of the relevant aerodynamics integrated with my experience as a soccer player.

Ballistics is the study of objects flying through the air, one that has received considerable attention owing to its military applications. We begin by considering the simplest possible theoretical description of a football in flight, that of a sphere of mass m flying through a vacuum, in which there is no aerodynamic influence on the motion, a classic high school physics problem. The trajectory of the ball $\mathbf{x}(t) = (x(t), z(t))$

can be simply expressed through Newton's first law:

$$m\ddot{\mathbf{x}} = -m\mathbf{g} \; , \tag{1}$$

where $\mathbf{g} = -g\hat{\mathbf{z}}$ is the acceleration due to gravity. This equation may be solved subject to the initial conditions $(x, y) = (0, 0)$ and $(\dot{x}, \dot{z}) = (U_0 \cos\theta, U_0 \sin\theta)$, where θ is the initial take-off angle and U_0 the initial speed. Doing so yields the trajectory $(x(t), z(t)) = (U_0 \cos\theta t, U_0 \sin\theta t - \frac{1}{2}gt^2)$. As indicated by the uppermost curve in Figure 1, this trajectory is symmetric, with the second half of its trajectory being the mirror image of its first. Setting $z = 0$ indicates that the time of flight is $t_f = 2U_0 \sin\theta/g$. The range of the ball is thus $x(t_f) = U_0^2 \sin 2\theta/g$, and achieves a maximum of U_0^2/g with a take-off angle of $\theta = 45°$.
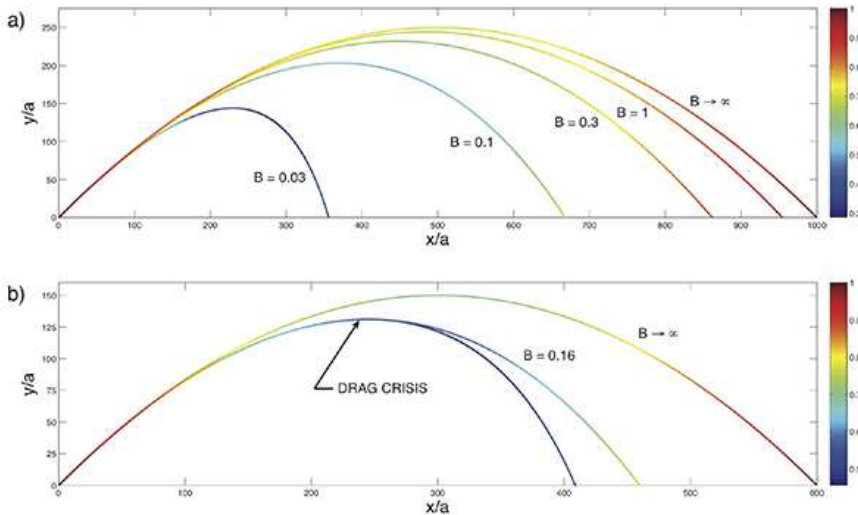

Figure 1: Computed trajectories of non-spinning balls. a) Trajectories of football-sized balls launched at an angle of $45°$ and an initial speed of 32 m/s (corresponding to $A = U_0^2/(ga) = 910$; see Figure 2) with different coefficients of ballistic performance, $B = gm/(\pi a^2 \rho U_0^2)$. The instantaneous flight speed is prescribed by the color of the curve, and the coordinates scaled by the ball size a. In the limit of $B \to \infty$, aerodynamic effects are negligible: the range is a maximum, and the flight path symmetric about its mid point. As B is decreased progressively, the range is decreased in response to aerodynamic drag, and the symmetry of the trajectory is broken: the ball falls more slowly and more steeply than it rises. b) Computed trajectories of footballs in a vacuum (upper curves) and in standard atmospheric conditions. Balls are launched with initial velocity of 25 m/s (corresponding to $A = 550$, $B = 0.16$) and take-off angle of $45°$. The lower curve indicates the influence of the drag crisis: at $Re = 10^5$, the ball decelerates through the drag crisis, and the drag coefficient C_D increases from 0.1 to 0.4. The resulting increase in drag is reflected in the decreased range and heightened asymmetry of the trajectory. Image courtesy of Dan Harris.

The characteristic release speed of a well struck goal kick is approximately 30 m/s. Kicking a soccer ball at this speed at the optimal angle of 45° indicates a maximum range of 120 m, which is nearly twice that observed. Moreover, casual observation indicates that the average goal kick violates the symmetry of the predicted trajectory, with the ball falling more steeply than it climbs. Experienced players know that the range of a goal kick may be extended by imparting backspin to the ball, and that 45° is not necessarily the optimal launch angle. Finally, it is common for long kicks to stray from a vertical plane. None of these features can be rationalized without considering the influence of the ambient air on the flight of the ball.

Quite generally, an object moving at a speed U through a fluid experiences resistance that depends on the fluid properties, specifically its density ρ and dynamic viscosity μ (or alternatively, the kinematic viscosity, $\nu = \mu/\rho$). This resistance in general has two components, viscous drag and pressure (or 'form') drag. Flow of a fluid past a solid exerts a tangential stress (force per unit area) of $\mu U/a$, where U/a is the local shear on the solid's boundary. Consequently, we anticipate that the characteristic viscous drag on a sphere of radius a will be obtained by multiplying this characteristic viscous stress by the surface area of the sphere, $4\pi a^2$, thus yielding a viscous drag proportional to $D_v \sim \mu U \pi a$. The pressure drag arises from a pressure difference between the front and back of the ball. The magnitude of this pressure difference in general depends on the details of the flow, but typically scales as ρU^2. The resulting pressure drag is thus obtained by multiplying this pressure difference by the exposed area of the sphere, and so is proportional to $D_p \sim \rho \pi a^2 U^2$. The relative magnitudes of these characteristic pressure and viscous drags is given by the Reynolds number:

$$Re = \frac{\text{PRESSURE DRAG}}{\text{VISCOUS DRAG}} = \frac{U\,a}{\nu} \,. \tag{2}$$

The Reynolds number characterizing the flight of a number of sports balls is included in Figure 2. Note that the Reynolds number is high for all sports balls, and the largest for footballs owing to the relatively large speed and ball size.

The pressure drag is thus dominant for most sports balls, including footballs, and a good approximation for the drag is a force opposing motion with magnitude $C_D \rho U^2 \pi a^2/2$, where a is the ball radius, ρ is the air density, and U is the ball speed. The drag coefficient C_D is in general a function of both Re and surface roughness, but is an order 1 constant at the high Re appropriate for ball sports. The empirical dependence of C_D on Re has been well characterized for a smooth ball, for which $C_D \sim 0.4$ for $10^3 < Re < 2 \times 10^5$ (Smith $et\ al.$, 1999). As Re is further increased, C_D decreases dramatically to a value of approximately 0.1 before recovering to a value of approximately 0.4 for $Re > 10^7$. This precipitous drop in C_D, termed the drag crisis, plays a critical role in many ball sports (Mehta 1985, Mehta & Pallis 2001), including football. The critical Reynolds number Re_c at which the drag crisis arises varies from sport to sport, as it is strongly influenced by the ball's surface roughness. For example, the dimples on a golf ball prompts the drag crisis at $Re_c = 5 \times 10^4$, the

paneling on a football at $Re_c = 10^5$, the corresponding speed being roughly 15 m/s.

Incorporating aerodynamic drag leads to an improved equation for the trajectory of a ball in flight. Denoting the position of the ball's center by $\mathbf{x}$ and its velocity by $\dot{\mathbf{x}} = \mathbf{U} = U\hat{\mathbf{s}}$, we augment (1) to deduce:

$$m\ddot{\mathbf{x}} = m\mathbf{g} - C_D \frac{\pi a^2}{2}\rho|\dot{\mathbf{x}}|^2\hat{\mathbf{s}} \,, \tag{3}$$

where we again stress that the drag coefficient C_D depends in general on both $Re = Ua/\nu$ and the sphere's surface roughness. Nondimensionalizing (3) on the basis of the a lengthscale corresponding to the ball radius a, a velocity scale U_0 and a timescale a/U_0 yields a dimensionless trajectory equation for the dimensionless ball position $\mathbf{X} = \mathbf{x}/a$:

$$A\ddot{\mathbf{X}} = \hat{\mathbf{z}} - \frac{C_D}{2B}|\dot{\mathbf{X}}|^2\hat{\mathbf{s}} \,. \tag{4}$$

Two dimensionless groups appear. We refer to the first, $A = U_0^2/(ga)$, as the range parameter, which indicates the relative magnitudes of the maximum range of the ball in vacuo, U_0^2/g, and the ball radius a. We refer to the second as the coefficient of ballistic performance:

$$B = \frac{\text{WEIGHT}}{\text{AIR DRAG}} = \frac{mg}{\pi\rho a^2\, U_0^2} \,, \tag{5}$$

which indicates the relative magnitudes of the ball's weight and the aerodynamic drag force at launch. The ballistic performance indicates how important aerodynamic forces are on the trajectory of a ball in flight. B values for a number of common ball games are listed in Figure 2. Note that aerodynamic forces are most important for light balls: it is thus that one can throw a golf ball much farther than a ping pong ball.

Figure 1a indicates the trajectories computed from (4) using the same release speed ($U = 32$ m/s, corresponding to $A = 910$) and launch angle, $45°$, for balls with different B values. For high B, the trajectory is virtually unaffected by aerodynamic effects, and so follows a nearly parabolic trajectory. Such is the case for the shot put. Conversely, for small B values, aerodynamic forces lead to a rapid deceleration of the ball, and a striking asymmetry in the ascending and descending portions of the trajectory; specifically, the ball speed decreases rapidly, and falls relatively steeply from the apex of its trajectory. One can thus rationalize the asymmetric trajectory of goal kicks in football, which reflects the influence of aerodynamic drag. Incorporating air drag reduces B from ∞ to 0.1 for the case of a football in flight, and so reduces the predicted range of goal kicks from 120 m to 60 m, which is more consistent with observation. Figure 1b indicates the influence of aerodynamic drag on the flight of a football struck at 25 m/s. Once again, the range is reduced by the incorporation of air drag. The lower curve indicates the influence of the drag crisis (to be discussed in § 3),

which further reduces the range, and heightens the asymmetry of the trajectory. As we shall see, consideration of the influence of air on the football not only allows us to improve our estimate for the range of a goal kick, but to rationalize the motion of the ball out of the vertical plane, the anomalous curvature of spinning and non-spinning balls in flight.

2   The equations of fluid motion

While we have already demonstrated the importance of air drag in rationalizing the range of a football, it is important to understand its origins if we are to come to grips with more subtle aerodynamic effects such as the Magnus and reverse Magnus effects. Just as Newton's Laws describe the motion of discrete particles, Navier-Stokes equations describe the motion of an incompressible fluid of constant density ρ and viscosity $\mu = \rho\nu$ in the presence of a gravitational field $\mathbf{g}$. The velocity $\mathbf{u}$ and pressure p fields within a fluid evolve according to

$$\rho\left(\frac{\partial \mathbf{u}}{\partial t} + \mathbf{u}\cdot\nabla\mathbf{u}\right) = -\nabla p_d + \rho\nu\nabla^2\mathbf{u} \quad , \quad \nabla\cdot\mathbf{u} = 0 \, , \tag{6}$$

where $p_d = p - \rho g z$ is the dynamic pressure (Acheson 1990). The fluid momentum may change as a result of inertial forces, dynamic pressure gradients within the fluid, and viscous stresses, which act everywhere to suppress velocity gradients and so resist motion. Equation (6) is a formidable equation that can only be solved exactly for some very simple flows, the high Re flow around a football not being one of them. We thus proceed by assessing the relative magnitudes of the terms in (6), with hopes that some of them will be negligibly small.

Consider a sphere of radius a moving through a fluid at speed U. We define dimensionless (primed) quantities in terms of dimensional ones:

$$\mathbf{u}' = \mathbf{u}/U \quad , \quad \mathbf{x}' = \mathbf{x}/a \quad , \quad t' = tU/a \quad , \quad p' = p/(\rho U^2) \, . \tag{7}$$

Rewriting (6) in terms of these dimensionless variables and dropping primes yields

$$\frac{\partial \mathbf{u}}{\partial t} + \mathbf{u}\cdot\nabla\mathbf{u} = -\nabla p_d + \frac{1}{Re}\nabla^2\mathbf{u} \, , \tag{8}$$

where we again see the emergence of the Reynolds number $Re = Ua/\nu$. We have seen previously that the characteristic Re of a football in flight is in excess of 10^4, and so might feel justified in neglecting the final term in (6), that represents the viscous stresses within the fluid. We would thus obtain the Euler equations that describe the flow of inviscid fluids:

$$\frac{\partial \mathbf{u}}{\partial t} + \mathbf{u}\cdot\nabla\mathbf{u} = -\nabla p_d \quad , \quad \nabla\cdot\mathbf{u} = 0 \, . \tag{9}$$

In the limit of steady flow, as one might expect to arise for a ball flying through the air at uniform speed, (8) may be expressed as

$$\nabla \left(p + \frac{1}{2}\rho u^2 \right) = 0 \; : \tag{10}$$

along a streamline of the flow, $p + \frac{1}{2}\rho u^2 =$ constant, a result known as Bernoulli's Theorem. If the flow speed increases along a streamline, the pressure necessarily decreases, and vice versa.

Sport	m (g)	a (cm)	U_0 (m/s)	Re	A	B	S
Shot put	7260	6	10	40,000	170	54	0.05
Basketball	630	11.9	15	120,000	190	0.5	0.07
Tennis	58	3.8	70	180,000	12,000	0.22	0.19
Cricket	160	3.6	40	100,000	4,400	0.2	0.18
Baseball	150	3.66	40	100,000	4,200	0.2	0.05
Football	430	11.3	32	240,000	910	0.1	0.21
Golf	45	2.1	80	110,000	30,500	0.05	0.09
Volleyball	270	10.5	30	210,000	860	0.08	0.21
Squash	24	2.0	70	100,000	24,500	0.03	0.1
Ping-pong	2.5	2	45	60,000	10,125	0.008	0.36

Figure 2: The physical parameters of many common ball sports: a and m correspond to the ball's radius and mass, respectively, U_0 to its peak speed, Ω its spin angular velocity, and $\nu = 0.15$ cm^2/s to the kinematic viscosity of air. The corresponding dimensionless groups: the Reynolds number, $Re = U_0 a/\nu$, the range parameter $A = U_0^2/(ga)$, the coefficient of ballistic performance, $B = mg/(\pi a^2 \rho U_0^2)$ and the spin parameter $S = \Omega a/U_0$. The range parameter A indicates the relative magnitudes of the ball's maximum range in vacuo and its radius. The lower B, the greater the influence of aerodynamic effects on the flight of the ball. The small values of B for most ball sports indicate that the aerodynamic drag exerted at peak speed is typically comparable to or greater than the weight of the ball.

D'Alembert's Paradox is the inference that the drag on a body moving steadily through an inviscid fluid must vanish (Batchelor, 1967). This may be seen simply for the case of a spherical object: since the streamlines computed for inviscid flow around a sphere are fore-aft symmetric, so too must be the pressure distribution. As the drag on the sphere in the high Re limit is deduced by integrating the fluid pressure over the sphere, this calculation indicates zero drag. We have already stated that the

aerodynamic drag on balls in flight is non-zero, of order $\pi a^2 \rho U^2$, so what have we missed?

3 Boundary layers

The complete neglect of viscous effects is an untenable approximation, even in the limit of exceedingly large Re, as it gives rise to a number of conceptual difficulties, including D'Alembert's Paradox. While viscosity is negligible on the scale of the flow around the ball, it becomes significant in a thin boundary layer of thickness δ adjoining the ball. Within the boundary layer, viscous forces $\mu \nabla^2 \mathbf{u} \sim \mu U/\delta^2$ are comparable to inertial forces $\mathbf{u} \cdot \nabla \mathbf{u} \sim U^2/a$, the balance of which indicates a boundary layer thickness $\delta \sim a \, Re^{-1/2}$. As evident in Figure 2, Reynolds numbers are high in all ball sports, so the corresponding boundary layers are thin. In football, for example, the characteristic boundary layer thickness is $\delta \sim 0.1$ mm.

How is it that incorporating viscosity can give rise to a drag force of order $\rho U^2 \pi a^2$ that does not depend explicitly on viscosity? The influence of the viscous boundary layer is twofold. First, it ensures that there will always be some non-zero drag on an object through the influence of viscous stress. For high Re flow past an object, the viscous drag per unit area generated within its boundary layer, or skin friction, scales as $\mu U/\delta$. Thus, the characteristic viscous drag acting on a ball in flight will scale as $\mu U \pi a^2/\delta$. For the Reynolds numbers appropriate for most sports balls (Figure 2), this viscous contribution to the total drag is negligible. The dominant effect of the viscous boundary layer is to initiate boundary layer separation, thus breaking the symmetry of the flow and giving rise to a non-zero pressure drag of order $\rho U^2 \pi a^2$.

Flow past a smooth, rigid sphere is a canonical problem that has been studied exhaustively both experimentally and theoretically (Shapiro 1961, Smith *et al.* 1999). At low Re, the flow is dominated by viscous stresses, and the streamlines are symmetric fore and aft of the sphere (Figure 3a). The drag on the sphere, $D = 6\pi\mu U a$, increases linearly with both the flow speed U and the fluid viscosity. The flow remains viscously dominated until $Re \sim 1$, when inertial drag associated with a fore-to-aft pressure drop becomes significant. At $Re = 10$, a laminar ring vortex is established downstream of the sphere (Figure 3b). For $Re > 100$, this vortex becomes unstable, and the resulting time-variation in the downstream pressure field gives rise to a lateral force on the ball (Figure 3c). In a certain regime, the vortex peals off the back of the ball like a helix; consequently, the sphere proceeds in a spiraling fashion. This transition from rectilinear to helical motion may be observed in fireworks, and also in your local bar. For similar reasons, champagne bubbles rise in straight lines (Liger-Belair, 2004), while their relatively high-Re counterparts in a beer glass spiral as they rise.

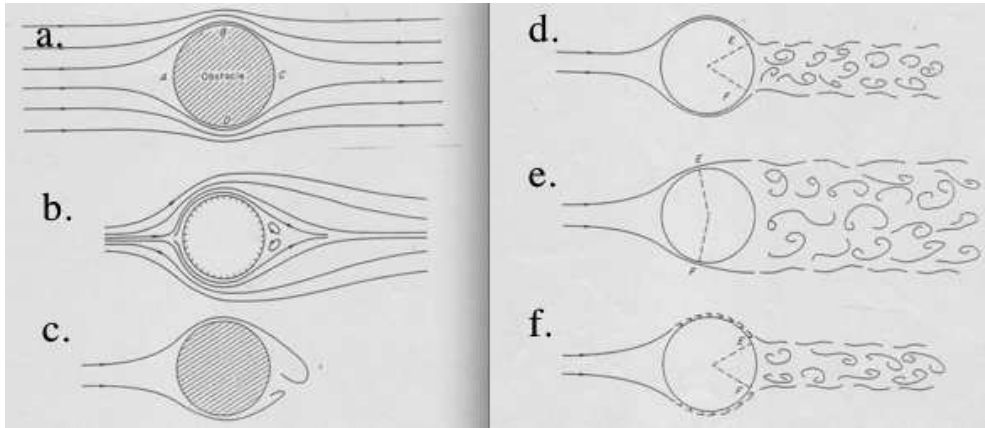As Re is further increased, the flow in the wake becomes progressively more com-

Figure 3: Schematic illustration of the evolution of the flow past a smooth sphere with increasing Reynolds number, $Re = Ua/\nu$. a) For $Re \ll 1$, the streamlines are fore-aft symmetric and the drag is principally of viscous origins. b) For $Re > 10$, boundary layer separation downstream of the sphere induces a vortical wake and a significant pressure drag. c) For $100 < Re < 1000$, the vortical wake becomes unstable, resulting in lateral forces on the sphere. d) For $Re > 1000$, the wake becomes turbulent, its extent being maximum for e) $Re \approx 2 \times 10^5$. f) For $Re > 2 \times 10^5$, the boundary layers become turbulent, delaying the boundary layer separation and decreasing the extent of the turbulent wake. Owing to the resulting dramatic reduction in drag on the sphere, the latter transition is called the drag crisis. Note that the precise Re-values at which flow transitions occurs depends strongly on the sphere's surface roughness. Images from Daish (1972).

plex until achieving a turbulent state (Figure 3d). Then, the pressure in the wake is effectively uniform, and determined by the pressure in the free stream at the point of separation of the wake. As Re increases, this point of separation generally moves upstream towards the equator of the sphere. Thus, the pressure in the wake decreases, while the area of the wake increases, the net effect being a drag that increases monotonically with Re. Finally, when the separation line reaches the equator, the drag on the sphere achieves its maximum, as the pressure drop fore-and-aft is maximum, as is the area over which the anomalous pressure low in the wake acts (Figure 3e). In this configuration, it is simple to make a reasonable estimate for the fore-aft pressure drop, which should correspond to the pressure drop along the streamline passing from the upstream stagnation point to the equator, $\rho U^2 a^2/2$, according to Bernoulli's Theorem. Further increasing Re beyond a critical value of 2×10^5 on a smooth ball prompts the drag crisis, at which the drag drops drastically, typically by a factor of 3 (Figure 3f). Here, the boundary layer on the leading face of the sphere becomes turbulent, the effect being to displace the point of boundary layer separation downstream, and so reduce the drag. This delay in the boundary layer separation may be understood as being due to the boundary layer turbulence mixing high-momentum

fluid down from the laminar external flow (Shapiro 1961).

The sensitivity of the aerodynamic force to the drag crisis plays a critical roll in a number of ball sports. The progression detailed in Figure 3 is that observed on a smooth ball; however, the progression is qualitatively similar on rough balls. Most sports balls have some roughness elements, either fuzz in the case of tennis balls (Mehta *et al.* 2008), stitches in the case of cricket (Mehta *et al.* 1983, Mehta 2005) and baseballs (Nathan 2008), or dimples in the case of golf balls (Erlichson 1983). For all such balls, the roughness serves to encourage turbulent rather than laminar boundary layers, so that the drag crisis is achieved at lower speeds, and the drag greatly decreased. As previously noted, the drag crisis arises at $Re \approx 2 \times 10^5$ on a smooth ball, $Re \sim 10^5$ for footballs and $Re = 3 \times 10^4$ for golf balls, whose range is thus doubled by the presence of the dimples. Controlled orientation of the stitches on baseball and cricket balls gives rise to anomalous lateral or vertical forces owing to the asymmetry of the boundary layer separation on the ball's surface, an effect exploited by pitchers and bowlers, respectively (Mehta and Pallis 2001).

The stitching of footballs ensures that, at the peak speeds relevant for shooting, the boundary layer is typically turbulent. However, as the ball decelerates in response to aerodynamic drag, its Re likewise decreases, ultimately reaching the critical value of 10^5 at a speed of $U \sim 15$ m/s. It then crosses the drag crisis threshold from above, at which point its boundary layers transition from turbulent to laminar. Consequently, the drag increases by a factor of approximately 3, and the ball decelerates dramatically. On a goal kick or a free kick, this drag crisis typically arises during the descent phase; thus, it will amplify the asymmetry of the trajectories apparent in Figure 1a. The influence of the drag crisis on a ball struck at $U_0 = 25$ m/s is illustrated in Figure 1b. As we shall see in § 4, the drag crisis will have an even more striking effect on spinning balls in flight.

Finally, we note that the progression detailed in Figure 3 of flow past a sphere is qualitatively different for streamlined bodies. If a body is shaped like a modern airfoil or, for that matter, like a trout, one can avoid boundary layer separation entirely. In this case, the drag is prescribed entirely by the applied viscous stress or skin friction. As the Reynolds number increases, the boundary layer thickness scales like $\delta \sim a\, Re^{-1/2}$, and the skin friction like $\tau_s \sim \mu U/\delta$. The ratio of the skin friction drag τa^2 to the form drag associated with the fore-aft pressure drop across a bluff body, $\rho U^2 a^2$, is thus given by $Re^{-1/2}$. At the high Re appropriate for many modern sports, including ski racing and cycling, one can thus readily see the tremendous advantage of streamlining, now the basis for an enormous sports industry.

4   The effect of spin

4.1   The Magnus effect

The Magnus Effect is the tendency of a spinning, translating ball to be deflected laterally, that is, in a direction perpendicular to both its spin axis and its direction of motion. For example, if spin is imparted such that the angular velocity vector has a vertical component, the ball will be deflected out of the vertical plane depicted in Figure 1 by the Magnus force. The role of the Magnus effect on the flight of tennis balls was noted by Newton (1672), then again by Lord Rayleigh (1877), who remarked "...a rapidly rotating ball moving through the air will often deviate considerably from the vertical plane." The influence of spin on the flight of cannon balls was examined in 1742 by the British artillery officer Robins (1805). The effect takes its name from Professor Heinrich Gustav Magnus (1853), a physicist and chemist at the University of Berlin, who measured the lateral force on cylinders rotating in an air current. The first theoretical description of the effect was presented by Lord Rayleigh, whose theory predicted that the lift is proportional to the product of the speeds of rotation and translation. However, it was not until the theory of boundary layers, developed by Ludwig Prandtl (1904; see also Schlichting 1955, Anderson 2005), that the subtlety of the effect could be fully appreciated.
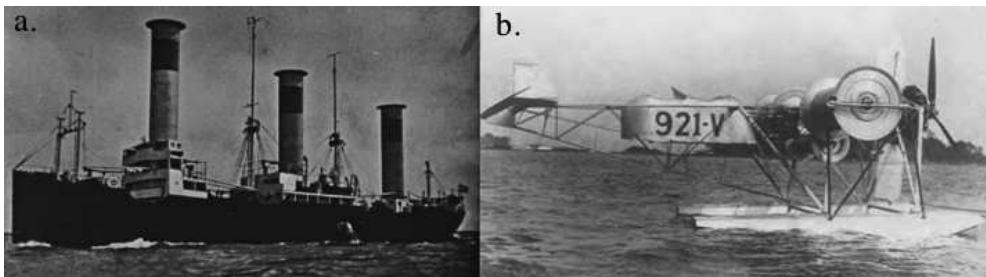

Figure 4: Two applications of the Magnus effect. a) The sail boat *Barbara*, conceived and built by Flettner in the 1920s, has sails with the form of spinning cylinders (Gilmore 1984). b) The rotorplane 921-V, whose wings take the form of spinning cylinders, was developed shortly thereafter (Anon. 1930). Magnus boats were more successful than their airborne counterparts; the former having circumnavigated the globe, the latter having only flown once before crash landing.

The Magnus effect has received considerable attention owing to its importance in ballistics. When cylindrical shells are fired from guns or cannons, they are often spin stabilized: rotational angular momentum imparted by fluting of the rifle shaft keeps the shells from tumbling in flight, thus maximizing their speed and range. When fired into a cross wind, or fired from a moving ship or plane, this spin interacts with

the translation of the shell to generate an anomalous lift force, that may cause the shell to miss its target. Ballistics experts and snipers are thus well aware of the Magnus effect and how to correct for it. The Magnus effect has inspired a number of inventions, some of them unlikely. The Flettner rotor is a sailboat whose sail is replaced by a rotating cylinder (Figure 4a). The motion of the cylinder is driven by a generator, and interacts with the wind to drive the boat forward via Magnus forces. The Flettner rotor boat has successfully circumnavigated the globe, and new styles of Magnus sailboats are currently being explored owing to their energy efficiency. More surprising still is the Magnus airplane, for which lift is generated by flow over wings comprised of rotating cylinders (Figure 4b). While the lift forces so generated may be higher than those generated by conventional airfoil wings, the relatively large drag induced by their cylindrical form makes this design impractical.

The Magnus effect is also exploited in a number of Nature's designs. Many seed pods, including maple keys, are shaped such that they tumble as they fall (Figure 5a; Vogel 2003). The coupling of the resulting rotational and translational motions can give rise to a Magnus lift force that considerably extends the range of these seed pods, thus giving them an evolutionary advantage. It has also been claimed that the range of the box mite, that rotates when it leaps, is increased by the Magnus effect (Figure 5b; Wauthy *et al.* 1998).
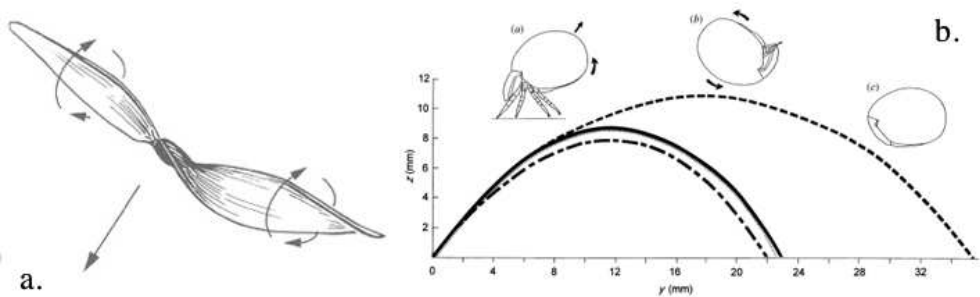

Figure 5: Two examples of the Magnus effect in the natural world. a) Many seed pods are shaped so as to tumble with backspin as they fall, thus extending their range via Magnus lift (Image from Vogel 2003). b) The box mite leaps with backspin, thus extending its range (Image from Wauthy *et al.* 1998).

For a ball in flight with velocity $\dot{\mathbf{x}} = \mathbf{U} = U\hat{\mathbf{s}}$ that is also spinning with angular velocity $\boldsymbol{\Omega}$, in addition to drag, there is thus a lift force in a direction perpendicular to both $\boldsymbol{\Omega}$ and $\mathbf{U}$. This so-called Magnus force takes the form $\mathbf{F_M} = C_L \pi \rho a^3 \, \boldsymbol{\Omega} \wedge \mathbf{U}$. We can thus augment (3) to deduce the trajectory equation for a translating, spinning

ball:

$$m\ddot{\mathbf{x}} = m\mathbf{g} - C_D \frac{\pi a^2}{2} \rho\, U^2\, \hat{\mathbf{s}} + C_L \pi \mathbf{a}^3 \rho\, \mathbf{\Omega} \wedge \mathbf{U} \ . \tag{11}$$

The lift coefficient C_L, like the drag coefficient C_D, is an order one constant that depends on both the Re and the sphere's surface roughness; furthermore, C_L depends on the spin parameter $S = \Omega a/U$, that prescribes the relative magnitudes of the ball's rotational and translational speeds. We note that in all sports, one may safely assume that $0 < S < 1$, as is evident in the estimates presented in Figure 2. As we shall see in what follows, the dependence of C_L on Re, S and the surface roughness is quite dramatic; for example, altering a ball's surface roughness can change the sign of C_L.

Bernoulli's Theorem provides a simple but ultimately unsatisfactory rationale for the anomalous trajectories of spinning balls in flight. Imagine a ball flying through the air with pure backspin or 'slice', so that its rotation vector $\mathbf{\Omega}$ is horizontal. Assuming that the spinning ball contributes a net circulation to the ambient flow, one expects the air speed to be larger on the upper, retreating surface than on the lower, advancing surface. Bernoulli's Theorem would thus indicate a vertical pressure gradient that will drive the ball upwards, consistent with one's intuition. This physical picture was developed formally by Lord Rayleigh (1877), who solved for inviscid flow around a two-dimensional translating spinning cylinder, the effect of the spin being incorporated by imposing a circulation $\Gamma = \Omega a^2$. His solution indicated that the effect of the circulation was to shift the stagnation points (and associated Bernoulli high pressure points) downwards from the leading and trailing edges of the circle, giving rise to an upward lift force per unit length of $\rho U \Omega a^2$ (Figure 6b). In what follows, we shall expose the shortcomings of this inviscid physical picture, demonstrating that the anomalous force may differ from that predicted by Lord Rayleigh not only in magnitude, but direction. In particular, the lift coefficient C_L depends not only on Re and S, but is likewise sensitive to the surface roughness in the parameter regime relevant to sports balls in flight.

4.2   The reverse Magnus effect

Having come to grips with the Magnus effect, and the traditional explanation thereof, one can only be puzzled to note that striking a smooth beach ball or an old, worn volleyball with spin has just the opposite effect: the ball bends in the opposite sense relative to a normal football, that is, $C_L < 0$. As we shall see, this arises due to the so-called reverse Magnus effect, a satisfactory explanation of which cannot be given in terms of Bernoulli arguments.

Figure 6a presents data collected from wind tunnel studies indicating the dependence of the Magnus force on both the translational and rotational speeds of a smooth cylinder, specifically, the dependence of the lift coefficient, $C_L = F_M/(\rho a^2 U \Omega)$, on the
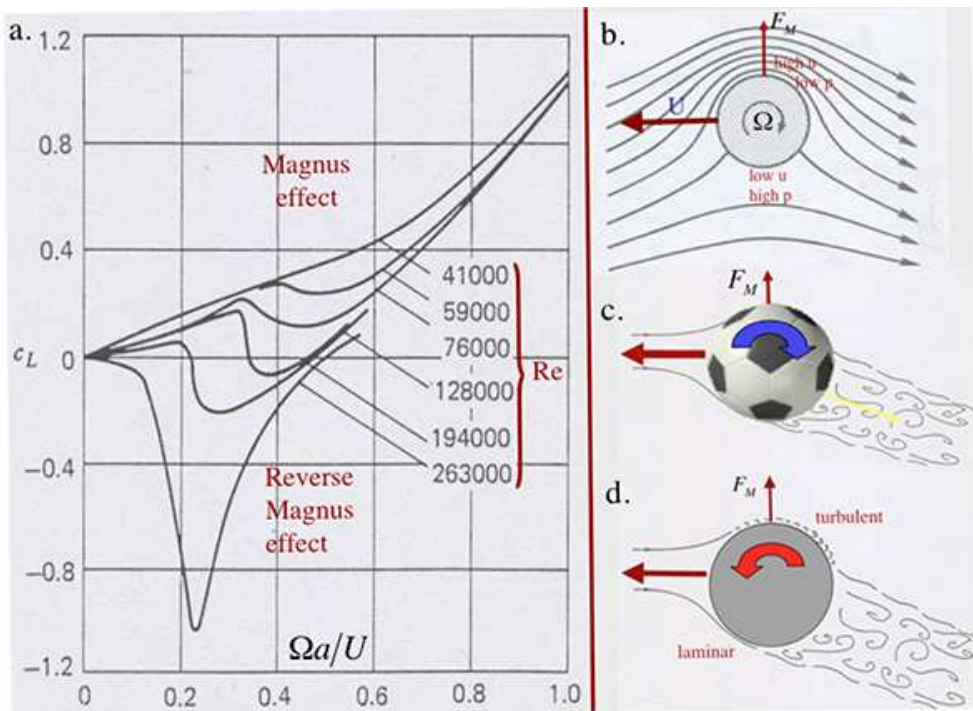
Figure 6: a) The dependence of the Magnus lift coefficient, C_L, on the translational and rotational speeds of a smooth cylinder. The Magnus force per unit length, $F_M = C_L \rho a^2 U \Omega$, where a is the cylinder radius, U its translational speed and Ω its rotational speed. At sufficiently high $Re = Ua/\nu$, we see that $C_L < 0$, indicating a reversal in the sign of the Magnus force. Image from Brown (1971), reprinted from Lugt (1995). b) The idealized picture of inviscid flow past a spinning cylinder, in which a circulation Ωa^2 is imposed on the streaming flow past the body. On the basis of this physical picture, Lord Rayleigh predicted $C_L = 1$. In reality, we see in a) a strong dependence of C_L on both Re and $S = \Omega a/U$, as is the case for spheres. c) For flow past a real football, backspin serves to deflect the flow in the wake downwards, giving rise to a net lift force on the ball. d) The reverse Magnus effect. On a smooth ball, the Magnus force may reverse sign, causing the ball to bend the wrong way. This results from the difference in the boundary layers on the advancing and retreating sides, the former being turbulent, the latter laminar.

Reynolds number, $Re = Ua/\nu$, and the spin parameter, $S = \Omega a/U$ (Brown 1971). For $Re < 100000$, the Magnus force is always positive ($C_L > 0$); however, for $Re > 128000$, the sign of the Magnus force reverses ($C_L < 0$) over a finite range of rotation rates. This reversal of the direction of the rotation-induced force on a translating sphere is known as the reverse Magnus effect, and is most likely to arise at very large Re. While such a comprehensive data set has not been produced for spheres, the reversal of the

sign of C_L at high Re has also been reported (Maccoll 1928, Davies 1949, Barkla *et al.* 1971). The resulting reverse Magnus effect may be rationalized through our discussion in § 3 of boundary layers.

Owing to the different local speed difference between the ambient air and points on the surface of a translating, rotating sphere, the effective Reynolds numbers are different on the advancing and retreating sides of a spinning ball, which may result in two effects. When the boundary layers on both sides are either subcritical or supercritical, reference to Figure 3 indicates that the flow on the advancing side will separate sooner (nearer to the equator) than on the retreating side. The net effect will thus be a deflection of the wake towards the advancing side. For example, for a ball struck with pure backspin, this differential boundary layer separation will result in the wake being deflected downwards, the resulting force on the ball being upwards, as follows from the conservation of momentum (Figure 6c). The resulting force on the spinning ball is thus consistent with that predicted by the inviscid description of the Magnus effect (Figure 6b), but in reality relies critically on a difference in the geometry of boundary layer separation on the advancing and retreating sides of the ball.

We have seen that during the course of a typical shot, the ball decelerates through the drag crisis, its boundary layers transitioning from turbulent to laminar. When the ball is spinning, one expects the drag crisis to be crossed first on the retreating side, where the velocity difference between ball and free stream is minimum. There would thus arise a situation in which the boundary layer is turbulent on the advancing side, and laminar on the retreating side. The resulting delay of boundary layer separation on the advancing side would lead to an asymmetric wake, with air in the wake being deflected in the direction of the retreating side, giving rise to the reverse Magnus effect, and a lift force opposite that expected ($C_L < 0$; Figure 6d). As the ball decelerates further, both boundary layers will transition to laminar, and the lift anticipated on the basis of the traditional Magnus effect ($C_L > 0$) will be restored. To summarize, as a typical shot decelerates through the drag crisis, its Magnus force will change sign twice, as the retreating and advancing boundary layers transition in turn from turbulent to laminar.

The critical role of surface roughness on the Magnus effect is illustrated in Figure 7. A smooth plastic ball (similar to a beach ball) is struck with the instep in such a way as to impart typical spin (with the angular velocity vector $\mathbf{\Omega}$ vertical). Its trajectory is marked with blue circles. If it were a regular football, the ball would curve towards the shooter's left in response to the Magnus force; however, because it is smooth, the reverse Magnus effect applies, and the ball curves towards the shooter's right. The red trajectory indicates the trajectory of the same ball struck in precisely the same way; however, this time a single elastic band is wrapped around the ball's diameter. This rubber band is sufficient to ensure turbulent boundary layer separation on both sides of the spinning ball, so that the regular Magnus effect arises. The ball with the rubber band thus responds to rotation as does a regular football, and swerves to the

shooter's left.

We thus see the critical role of surface roughening on the flight of the football. It is noteworthy that, since the inception of the sport, footballs have always had significant roughness, first in the form of stitched seams between panels. Moreover, the shape of these panels has changed dramatically (Figure 8). The aerodynamic performance of a number of recent panel patterns has been investigated by Alam *et al.* (2011), who demonstrate that, while the ball's aerodynamic performance is sensitive to the presence of panels, it is not greatly altered by their particular form. In modern times, when it is entirely possible to produce a perfectly smooth ball, manufacturers choose not to do so for an obvious reason: the ball would, over a greater range of parameters, bend the wrong way.

5   Brazilian Free Kicks

Just as the Canadian Inuit are alleged to have hundreds of words for snow and ice, the Brazilians have an entire lexicon devoted to different styles of free kicks. We proceed by rationalizing the anomalous motion of each of the different styles in terms of the aerodynamics of balls in flight. The Chute de Curva describes classic bending of the ball, the simplest in terms of execution. For a right footer, one strikes the ball with the instep, sweeping the foot past as one does so, thus imparting a counterclockwise spin as viewed from above, a vertical Ω. In response, the ball 'bends' to its left as it flies through the air (Figure 6). The change in trajectory can be significant, with the ball moving laterally several meters during flight.

The Trivela (or 'Tres Dedos') is instead struck with the outside of the foot, with one's three outer toes as suggested by its name. This imparts the opposite spin to the ball, which thus (for a right footer) curves in the opposite direction, to the shooter's right. Owing to the decreased contact area during the foot strike, the trivela is generally more difficult to control than the Chute de Curva. The most celebrated trivela is undoubtedly that of Roberto Carlos in 1997 in the Tournoi de France, struck in a friendly against France from a distance of 37 meters (Dupeux *et al.* 2010). Careful viewing indicates that, had the ball followed its initial trajectory, it would have crossed the goal line roughly on the edge of the 18 meter box. However, owing to the spin-induced curvature of its flight, it nipped just inside the post, past an astonished french keeper.

The Folha Seca is struck with nearly pure topspin by brushing over the ball during the strike. As its name suggests, the ball then dips dramatically, falling like a dead leaf. While volleying a ball with topspin is relatively straightforward, imparting pure topspin is extremely difficult to do from a dead ball, and only a few players have truely mastered it. The Brazilian old-timers speak of Didi as its inventor, while Juninho Pernambucano and Cristiano Ronaldo are perhaps its best modern practitioners. The
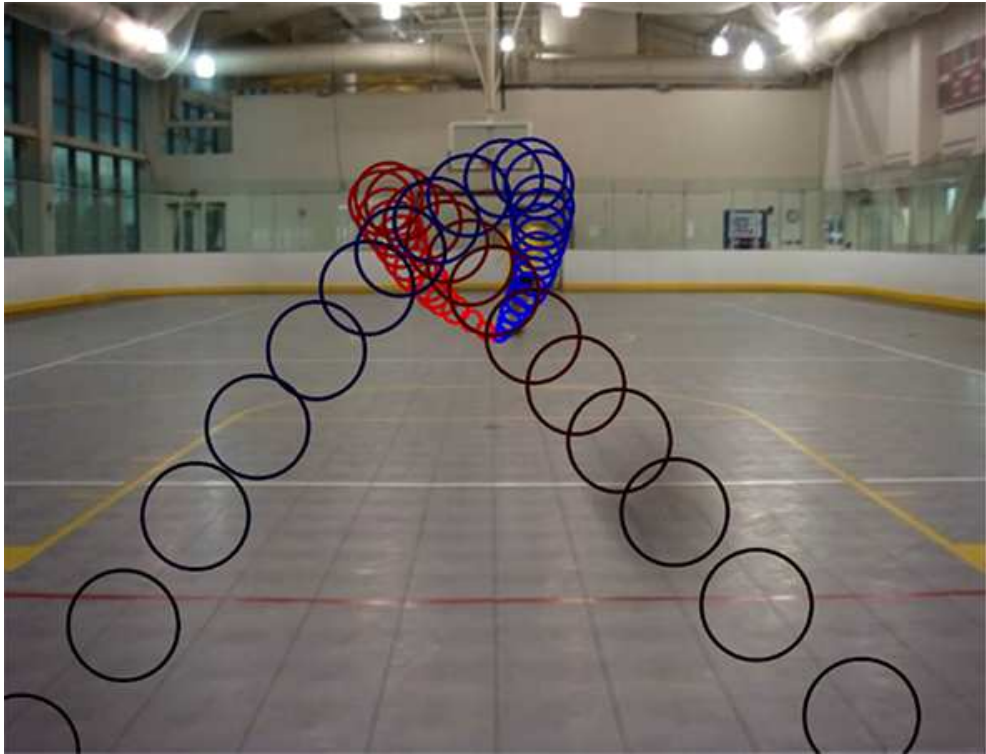
Figure 7: The trajectories of two nearly identically struck balls, one smooth, the other rough, the former responding to the reverse Magnus effect, the latter, the Magnus effect. The ball consists of a smooth beach ball. When struck with the right instep so as to impart rotation in the usual sense, it bends anomalously, from the shooter's left to right. Adding an elastic band around its equator is sufficient to render the boundary layer turbulent, therefore restoring the expected curvature, from the shooter's right to left. Thanks to Karl Suabedissen for his sniper-like precision, and Lisa Burton for her skillful ball tracking.

most visually striking shot in football deserves its colorful brazilian name, the Pombo Sem Asa. Struck hard and clean with no spin imparted at impact, the ball rockets through the air, moving erratically up and down, from side to side, like a Dove Without Wings. Its unpredictability renders it fearsome for goalkeepers, who find it extremely difficult to judge. Many free-kick specialists believe that both the Folha Seca and the Pombo Sem Asa are best induced by striking the ball's valve.

While four free kick styles are enumerated above, there are only two physical effects that need to be understood to rationalize them. The Magnus effect allows one to rationalize the lateral curvature of both the Chute de Curva and the Trivela, as well

Figure 8: The evolution of the football. While the form of the ball's paneling has changed significantly, surface texture remains a part of the modern ball. While modern fabrication techniques could create a smooth ball, the surface roughness is necessary to ensure that the ball maintains its aerodynamic properties, including its response to induced spin. Images compiled from various on-line sources.

as the anomalous dip of the Folha Seca. The aerodynamic origins of the unpredictable trajectory of the Pombo Sem Asa are more subtle. We have seen that as a ball passes through the drag crisis, the sign of the lift force is expected to change twice as the retreating and advancing sides of the ball transition in turn from turbulent to laminar. If the shot changes direction more than twice, then an alternate mechanism must be sought. One with the most likely candidate is the knuckling effect prevalent when baseballs are thrown with very little spin (Mehta and Pallis, 2001). Here, the orientation of the flow in the turbulent wake changes slowly in response to the slowly changing orientation of the seams. As each vortex shed in the wake of the ball represents a pressure anomaly, the changes in the vortex distribution are reflected in a time-varying aerodynamic force on the ball and an unpredictable trajectory. Despite the absence of pronounced seams on a volleyball, a similar knuckling effect arises when the ball is struck with very little spin (Mehta & Pallis, 2001).

6   Discussion

We have presented a rather idiosynchratic review of the dynamics of footballs in flight, highlighting the dominant influence of aerodynamics on their trajectories. We have seen that the interaction of surface roughness and boundary layer flows is critical in many aspects of football dynamics. Specifically, it prescribes both the aerodynamic drag on the ball, and so the range of goal kicks, as well as the anomalous lateral forces acting on rotating or non-rotating balls in flight. The Magnus effect allows one to rationalize the anomalous curvature of spinning balls, including the extended range of goal kicks struck with backspin, and the bending of free kicks around or over a wall of defenders with the Chute de Cura or Folha Seca, respectively.

We have elucidated the relatively complex physics behind the fact that the aerodynamic drag acting on a football in flight is proportional to $\rho U^2 \pi a^2$, and may be understood as being due to a pressure difference of order ρU^2 between the leading and trailing sides of the ball induced by boundary layer separation. The fact that this drag depends on the air density ρ suggests a dependence of the ballistic performance on the atmospheric conditions. For example, at Mexico City, at an altitude of 2.2 km, the air density is roughly 80% that at sea level. Thus, a 25 m shot will arrive approximately 0.02 seconds sooner, during which time a goalie lunging at 10 m/s will cover a distance of 20 cm. One thus sees that playing at altitude gives an advantage to the shooter, and tends to favor high-scoring matches. Of course, this aerodynamic advantage may be more than offset by the cardiovascular penalties associated with playing at altitude.

We have reviewed the standard inviscid treatment of flow past a spinning cylinder, typically the rationale provided for the Magnus effect, and found it wanting. While it predicts the correct direction for the Magnus force (based on the intuition of the soccer or tennis player), we have seen that this result is purely fortuitous. Specifically, we have seen that the Magnus force on a smooth, light sphere may act in a direction opposite to that on a football, as may be readily observed by kicking a beach ball. The fact that the sign of the Magnus force can reverse on nearly identical spinning balls (Figure 7) highlights the critical role of surface roughness and boundary layers in the Magnus effect. We feel confident in predicting that, however much manufacturing techniques evolve, there will always be roughness elements on the football; otherwise, players will have to adjust to the reverse Magnus effect.

We have reviewed the brazilian lexicon of free kicks, and provided rationale for the behaviour of each. The bulk can be understood simply in terms of the Magnus effect, the exception being the Pombo Sem Asa, which is struck without spin. Two possible rationale for the resulting irregular trajectory have been proposed. The first would indicate that the Pombo Sem Asa is the footballing equivalent of the knuckleball, its unpredictable trajectory due to the random shedding of vortices in its wake. Hong *et al.* (2010) performed windtunnel studies, in which the wake of the ball was visualized by dust placed on its surface. They note that the vortex shedding arises at a much

higher frequency than the directional changes of the ball, presumably owing to the significant influence of the ball's inertia. The second possibility is the double reversal of the sign of the lift force as a slowly spinning ball decelerates through the drag crisis. The relative importance of these two effects in the erratic flight of the Dove Without Wings will in general depend on the ball's spin rate, but remains an open question.

Another important aspect of the dynamics of football that I have not touched upon is the striking of the ball. The contact time between foot and ball was measured by Nunome *et al.* (2012), and found to be approximately 10 ms; however, this value will in general depend on both the geometry of the foot strike, and the overpressure of the ball. FIFA stipulates that internal overpressures lie in the rather sizable range of 0.6 to 1.1 atm. Within this range, contact times vary by approximately 20%, being larger for the softer balls. The contact time will in general determine the ability of the shooter to control the ball. In particular, the longer the contact time, the more readily the shooter can impart spin to the ball when trying to bend it. Conversely, if the shooter wants to strike the ball without spin, and so produce a Pombo Sem Asa, it is advantageous to minimize the contact time. The latter is consistent with the fact that in attempting to generate such a knuckling effect, many free-kick specialists strike the valve side of the ball, where the ball is relatively stiff and uncompliant, so as to minimize contact time.

We can now apply what we have learned to the puzzling question that faced me as a player when, having grown accustomed to playing in Boston's hot, dry summers, I had to adjust to the wet, wintry pitches of England. It became immediately apparent that bending the ball in a controlled fashion was significantly more difficult in the English winter, at times virtually impossible. We can see now why such would be the case. The balls in England were often water-logged, thus heavier and more slippery, as well as overpumped. As a result, imparting controlled spin was more difficult. Moreover, the additional weight of the wet ball insured that its effective coefficient of ballistic performance was higher, so it would respond less to the Magnus force. I can thus rationalize why my first attempts to bend the ball at the Fitzwilliam College grounds flew scud-like, well wide of both the wall and the net, and why I was subsequently relegated to the role of fair-weather free-kick specialist.

Acknowledgements

References

[1] Acheson, D.J., 1990. *Elementary Fluid dynamics*, Oxford University Press, Oxford.

[2] Adair, R.K., 2002. *The physics of baseball* (Harper Collins, New York).

[3] Alam, F., Chowdhury, H., Moria, H. and Fuss, F.K., 2010. A Comparative Study of Football Aerodynamics, *Procedia Engineering*, **2**, 2443-2448.

[4] Anderson, J.D., 2005. Ludwig Prandtl's boundary layer, *Physics Today*, December 2005, 42–45.

[5] Anonymous, 1930. Whirling spools lift this plane, *Popular Science Monthly*, November 1930.

[6] Asai, T., Seo. K. Kobayashi, O. and Sakashita, R., 2007. Fundamental aerodynamics of the soccer ball, *Sports Engineering*, **10**, 101–110.

[7] Barkla, H.M. and Auchterloniet, L.J., 1971. The Magnus or Robins effect on rotating spheres, *J. Fluid Mech.*, **47**, 437–447.

[8] Batchelor, G.K., 1967. *An introduction to fluid mechanics*, Cambridge University Press: Cambridge.

[9] Brown, F.N.M., 1971. *See the wind blow*, University of Notre Dame, Indiana.

[10] Daish, C.B., 1972. *The physics of ball games*, (English Universities Press: London).

[11] Davies, J.M., 1949. The aerodynamics of golf balls, *J. Appl. Phys.*, **20**, 821–828.

[12] Dupeux, D., Le Goff, A., Quéré, D and Clanet, C., 2010. The spinning ball spiral, *New J. Physics*, **12**, 093004.

[13] Erlichson, H., 1983. Maximum projectile range with drag and lift with particular application to golf. *Am. J. Physics*, **51**(4), 357–362.

[14] Frolich, C., 1984. Aerodynamic drag crisis and its possible effect on the flight of baseballs. *Am. J. Physics*, **52**(4), 325–334.

[15] Gay, T., 2004. *Football physics: the science of the game*, Rodale Inc.: New York.

[16] Gilmore, C.P., 1984. Spin sail harnesses mysterious Magnus effect for ship propulsion, *Popular Science*, November 1984, p. 70–72.

[17] Goff, J.E. and Carré, M.J., 2010. Soccer ball lift coefficients via trajectory analysis, *Eur. J. Phys.*, **31**, 775-784.

[18] Goff, J.E., 2010. Power and spin in the beautiful game, *Physics Today*, July issue, p. 62-63.

[19] Goff, J.E. and Carré, M.J., 2012. Investigations into soccer aerodynamics via trajectory analysis and dust experiments, *Procedia Eng.*, **34**, 158-163.

[20] Hong, S., Chung, C., Nakayama, M. and Asai, T., 2010. Unsteady aerodynamic force on a knuckleball in soccer, *Procedia Eng.*, **2**, 2455-2460.

[21] Hong, S. and Asai, T., 2011. Aerodynamics of knuckling effect shot using kick-robot. *Int. J. Appl. Sports Sci.*, **23** (2), 406-420.

[22] Liger-Belair, G., 2004. *Uncorked: The science of champagne*, Princeton University Press, Princeton.

[23] Lugt, H., 1995. *Vortex flow in nature and technology*, Krieger Publishing Company: Malabar, Florida, USA.

[24] Magnus, G., 1853. Uber die Abweichung der Geschosse, und: Uber eine abfallende Erscheinung bei rotirenden Korpern, *Annalen der Physik*, **164**(1), 129.

[25] Maccoll, J.W., 1928. Aerodynamics of a spinning sphere, *J. R. Aeronaut. Soc.*, **32** (213), 777–798.

[26] Mehta, R.D., 1985. Aerodynamics of sports balls, *Ann. Rev. Fluid Mech.*, **17**, 151–189.

[27] Mehta, R.D., Bentley, K., Proudlove, M. and Varty, P., 1983. Factors affecting cricket ball swing, *Nature*, **303**, 787–788.

[28] Mehta, R.D., 2005. An overview of cricket ball swing, *Sports Eng.*, **4**, 181-192.

[29] Mehta, R.D. and Pallis, J.M., 2001. Sports Ball Aerodynamics: Effects of Velocity, Spin and Surface Roughness, in *Materials and Science in Sport*, Ed. S. Froes, p. 185-197.

[30] Mehta, R.D., Alam, F. and Subic, A. 2008. Review of tennis ball aerodynamics. *Sports Technol.*, **1**, 7–16.

[31] Mehta, R.D., 2009. Sports ball aerodynamics, in *Sport Aerodynamics*, Ed. H. Norstrud, Springer: New York.

[32] Nathan, A.M., 2008. The effect of spin on the flight of a baseball, *Am. J. Phys.*, **76**, 119-124.

[33] Newton I., 1672. New theory of light and colours. *Phil. Trans. Roy. Soc. London* **1**, 678–688.

[34] Nunome, H., Shinkai, H., and Ikegami, Y., 2012. Ball impact kinematics and dynamics in soccer kicking, Proc. 30th Annual Conference of Biomechanics in Sports, Melbourne Australia.

[35] Prandtl, L., 1904. Uber Flussigkeitsbewegung bei sehr kleiner Reibung, in *Verhandlungen des dritten internationalen Mathematiker-Kongresses* Heidelberg, ed. A. Krazer (Teubner: Leipzig, Germany), p. 484.

[36] Rayleigh, Lord, 1877. On the irregular flight of a tennis ball. *Messenger of Mathematics.* **7**, 14–16.

[37] Robins, B., 1805. *New Principles of Gunnery*, ed. R. Hutton. First printed in 1742.

[38] Sakamoto, H. and Haniu, H., 1995. The formation mechanics and shedding frequency of vortices from a sphere in uniform shear flow, *J. Fluid Mech.*, **287**, 151–171.

[39] Schlichting, H., 1955. *Boundary-Layer Theory* (New York: McGraw-Hill).

[40] Shapiro, A.H., 1961. Shape and flow: The fluid dynamics of drag (Anchor Books: Boston).

[41] Smith, M.R., Hilton, D.K. and Van Sciver, S.W., 1999. Observed drag crisis on a sphere in flowing He I and He II, *Phys. Fluids*, **11**, 751–753.

[42] Vogel, S., 2003. *Comparative biomechanics: Life's Physical World*, (Princeton University Press: Princeton).

[43] Watts, R.G. and Sawyer, E., 1975. Aerodynamics of a knuckleball. *Am. J. Physics*, **43**(11), 960–963.

[44] Wauthy, G., Leponce, M., Banai, N., Sylin, G. and Lions, J.-C., 1998. The backwards jump of the box mite, *Proc R. Soc. Lond. B*, **265**, 2235–2242.

2 High jump and pole vault: a classical case of tunneling?

by A. Eddi
Physics of Fluids Group,
Faculty of Science and Technology and Mesa+ Institute,
University of Twente, 7500AE Enschede, The Netherlands

Abstract

High jumpers and pole vaulters are bending their bodies when clearing the bar. We will show that this effect allow them to maintain their center of mass lower than the bar, and thus clear a bar higher than expected. This can be ascribed to the deformability of their body which is not rigid but continuously changing shape during the jump. A physical analysis shows that they can improve their performance by a few centimeters using this technique and we will compare this prediction to actual championship data. We will also discuss the similarities and differences between this effect and quantum tunneling.

1 Introduction

High jump and pole vault are olympic sports from the start of modern Olympic Games in 1896. In both cases, the athlete has to clear a bar standing at a given height from the ground. After running a few meters, he/she exchanges his kinetic energy for potential energy, converting first the horizontal speed into vertical speed, and then experiencing a free flight.

The technique for high jump has considerably evolved from the beginning of this sport, progressively increasing the performances of the athletes. The scissors technique as well as the straddle technique have been progressively abandoned since the introduction by R. Fosbury of the upwards roll or Fosbury Flop (see fig. 1). This technical improvement allowed him to win the 1968 Olympics in Mexico, establishing a new olympic record (2.24 m). The current world record, 2.45 m, was established in 1993 by J. Sotomayor using this technique. The Fosbury flop is characterized by a large speed of the athlete at the end of a J-shaped run-up, but also by a large curvature of the body during the bar clearance. Is this bending just a consequence of the upwards roll, or does it provide a real advantage to the jumper?

To answer this question, we will base our analysis on actual data collected during championships [1, 2] and simple modeling that involves deformable body mechanics. We will show that the bending can enhance the performance of the jumper, as it allows him to "tunnel" through a potential barrier. We will look for evidence of such tunneling both in high jump and pole vault. Finally, we will present quantum tunneling and discuss the analogy between these two situations.
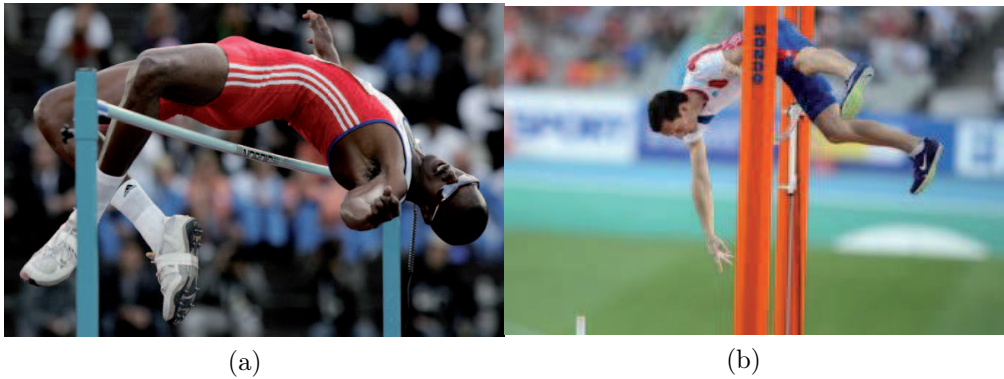
Figure 1: (a) Javier Sotomayor jumps using the Fosbury flop technique. (b) Renaud Lavillenie clearing a pole vault bar facing downwards. To what extend does the curvature of their bodies help them to clear the bar?

Athlete	V_0 (m.s^1)	V_z (m.s^1)	h_{pk} (m)
Conway	7.4	4.50	2.41
Forsyth	7.2	4.55	2.44
Partyka	7.6	4.50	2.39
Sjöberg	7.2	4.25	2.33
Sotomayor	8.0	4.6	2.46

Table 1: Conversion of horizontal velocity into vertical velocity and peak height for the 5 best high-jumpers at the 1992 Olympics in Barcelona. V_0 is the athlete's velocity before take-off, V_z his vertical velocity after take-off and h_{pk} the maximal height of his center of mass. Data from [2].

2   Physical approach

How high a living animal can jump? The jump requires a conversion of chemical energy into kinetic energy. The animal will contract its muscles, which are able to produce some mechanical work and this will set its body in motion. Provided that the resulting velocity is directed upwards, the body will rise and reach a maximal height. Using scaling arguments, it's possible to give a first order estimate of the typical height h it can raise [3, 4].

An animal, with a typical size L, has to produce a mechanical energy $E \sim L^3 h$ to reach the height h. This energy is provided by muscle contraction. This latter is made of N fibers, each of them providing a given elementary force. The number of fibers N typically goes as the section of the muscle L^2 The force F developed by a muscle being proportional to N, F scales, at first order, as the muscle section $F \sim L^2$

and will produce a work $W \sim F\Delta$, where Δ will denote the typical contraction of the muscle. Assuming, $\Delta \sim L$ (i.e. the contraction being proportional to the length of the muscle), we get $W \sim L^3$. By equating $E = W$, we notice that the height h reached by the animal doesn't depend on its size! This might explain why all animals, from grasshoppers to kangaroos, can jump over barriers with heights of the same order of magnitude, typically a meter. At second order, physiological characteristics must be taken into account: the design of the propelling member itself plays a major role in the amplitude of the jump.

2.1   Classical mechanics

Let us consider now a point-like mass m, thrown away with an initial velocity $\vec{V} = V_h \vec{e}_x + V_z \vec{e}_z$. Newton's law for motion gives a complete prediction of the parabolic trajectory followed by the mass during its free flight. By balancing the maximal gravitational potential energy acquired by the point-like mass at the top of the parabola with the vertical kinetic energy at take off, we can compute the value of the peak height of the trajectory h_{pk}:

$$h_{pk} = \frac{V_z^2}{2\,g}\ . \tag{1}$$

We can compare this prediction with the values obtained in [2], while measuring the kinematic parameters of the athletes who realized the five highest jumps during 1992 Olympics. All athletes have an horizontal velocity $V_0 \simeq 7.5$ m.s^{-1} during the last stride of their run-up, and convert it partially into vertical momentum during the take-off phase. They acquire a vertical velocity V_z ranging from 4.25 to 4.6 m.s^{-1}. At the top of their free flight, the experimental data show that the center of mass reaches a peak height h_{pk} in between 2.33 and 2.46 m. Taking into account the initial height of their center of mass (around 1.3 m at take-off), these values are in good agreement with the theoretical prediction given by eq. (1).

It is also worth noting that the jumper uses some internal energy to perform this conversion from horizontal to vertical impulsion. Indeed, the vertical speed at take-off V_z should rather be considered as the sum of two components: the first one is the vertical impulsion that a steady jumper can get just by using his leg as a spring; the second one is related to the actual conversion for horizontal speed into vertical speed. The jumper clearly uses these two aspects, optimizing the run-up but also converting some internal energy during the last stride in order to take-off vertically.

The same kind of simple energy argument can be applied for a pole vaulter [5]. Assuming that the athlete reaches the jumping point with an initial speed of 10 m.s^{-1} and that the pole allows him/her to convert all this kinetic energy into gravitational potential energy, we get a cleared height around 6 m, once again in good agreement

with the results obtained by the athletes (the outdoor world record by S. Bubka is 6.14 m).

Nevertheless, the case of athletic jumps (high jump, pole vault) should be treated with a more detailed model than this classical point-mass model. First, the athlete's body has a given thickness e, and this decreases the efficiency of his jump. It's also clear from the images that the jumper bends during his free flight (see fig. 1). We have to take into account the spatial extension of the athlete's body and predict the actual peak height of its center of mass as well as the cleared height. This bending might be an efficient mechanism to clear slightly higher bars, and then improve significantly the performance of the jumpers.

2.2   The rope model

We now model the athlete's body by a deformable rope, with a length L, and a constant mass per unit length λ. We will first look at the case where this rope can freely bend, without any maximal radius of curvature. For a rope which is not folded, its center of mass is located in the middle of the rope. If we now consider that it can wrap around the bar as soon as one of its extremities reach the bar, it will always maintain its center of mass under the bar level (see fig. 2(a)). Defining the cleared height h_{cl}, we can immediately show that $h_{cl} = h_{pk} + L/4$. This confirms that it can be useful for the athlete to bend his body!
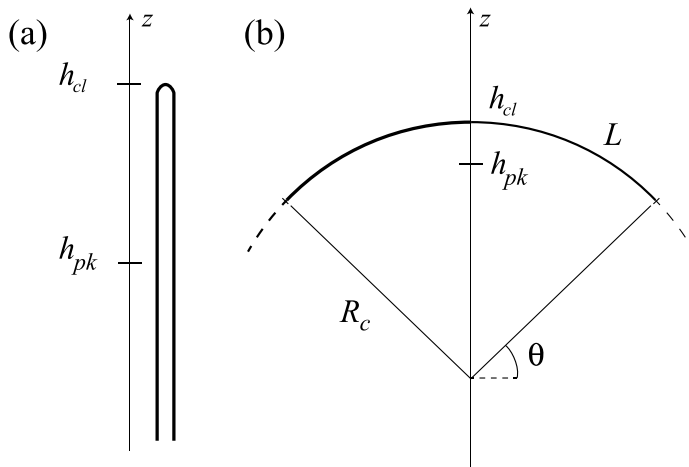

Figure 2: (a) Schematics of a freely bending rope over a bar. The peak height of the center of mass h_{pk} is lower than the cleared bar h_{cl}. (b) Rope with a length L and a minimum radius of curvature R_c. Again, h_{pk} is lower than h_{cl}.

A more reasonable model to mimic the physiology of human body is to consider that the rope can bend with a minimum radius of curvature R_c. We will consider that the rope has a circular shape with a radius R_c when it gets over the bar, and we impose that $L \leqslant \pi R_c$ so that the length of the rope is smaller than half the circle with radius R_c (see fig. 2(b)). We can compute the maximal height h_{pk} of its center of mass:

$$h_{pk} = \frac{2}{L} \int_\theta^{\pi/2} R_c^2 \sin\theta \, d\theta \ . \tag{2}$$

The calculation leads to

$$h_{pk} = \frac{2R_c^2}{L} \sin\frac{L}{2R_c} \ . \tag{3}$$

From this, we deduce the efficiency for clearing the bar with a circular rope Δh_{cl}:

$$\Delta h_{cl} = h_{cl} - h_{pk} = R_c \left(1 - \frac{2R_c}{L} \sin\frac{L}{2R_c} \right) \ . \tag{4}$$

Figure 3 show the efficiency Δh_{cl} as a function of the curvature $C = 1/R_c$ of the rope. Δh_{cl} increases monotonically with the curvature of the rope, being maximal when the rope has a semi-circular shape. In the opposite limit ($L \to 0$ or $R_c \to \infty$), we have $\Delta h_{cl} \to 0$. In that case, the result is the same as if the rope was a point-like mass or a rigid body.

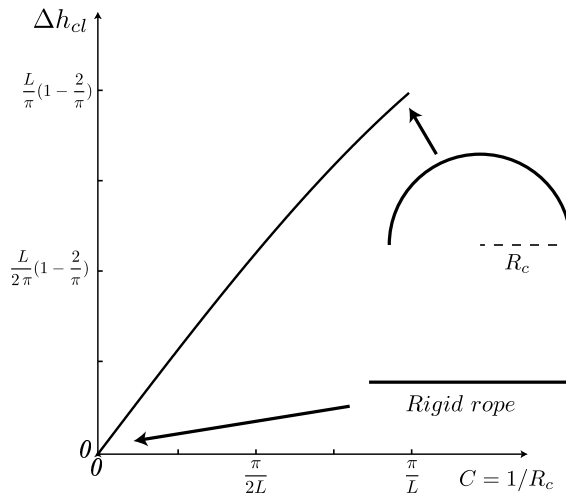Figure 3: Efficiency Δh_{cl} as a function of the curvature $C = 1/R_c$ of the rope. The efficiency increases monotonically with the curvature of the rope.

We conclude from this simplified model that the rope can get over the bar even if it's center of mass is always below the bar. This result is quite surprising, as it is in contradiction with the point-like mass description of the jump. This new feature is a consequence of the spatial extension of the rope, which allows this deformable body to adjust its mass distribution as it goes over the bar. Whatever the shape of the rope during the free flight, its center of mass will follow a parabolic trajectory. Nevertheless, our model demonstrates that the cleared height can be larger than the peak height h_{pk} of the center of mass.

3   High jump and pole vault

3.1   Bending of an athlete

Let us now consider the body mechanics of a real high jumper in more detail. Image processing allows for the reconstruction of the successive positions of the jumper in three dimensions [1, 2]. Figure 4(a) presents all these successive positions of a single jumper during one attempt. We clearly see that the athlete bends his body. The shape is approximately circular, which allows for using the previous rope model. Measurement of the body's radius curvature from this figure gives $R_c = 0.95 \pm 0.1$ m. According to our analysis and assuming that the jumper has a length $L = 1.8$ m, we deduce that the athlete's optimal efficiency is $\Delta h_{cl} \simeq 14$ cm. We also need to take into account the thickness e of his body, which decreases the absolute efficiency ζ,

$$\zeta = \Delta h_{cl} - e/2 , \tag{5}$$

of the jumper. Assuming $e = 20$ cm, our model predicts that the best bar that can be cleared by the jumper stands $\zeta \simeq 4$ cm above his center of mass.

If we now consider the case of a pole vaulter (see fig. 4(b)), this effect can be even larger. This is because the jumper wraps around the bar facing downwards, and thus bends in the natural direction for a human body. A rough analysis from fig. 4(b), and assuming a uniform mass distribution for the athlete, leads to an increased absolute efficiency $\zeta \simeq 20$ cm.

One can wonder why the high jumpers are using the Fosbury-flop technique rather than a technique in which they face downwards in order to maximize their efficiency. The Fosbury-flop seems to be the best compromise in between maximal kinetic energy at take off, efficiency in jump using the spring power of the leg and bending of the body. So far, this compromise is the best that has been found by the athletes, but we can still imagine that there could be another way to perform the inward roll allowing for a higher speed at take-off, thus optimizing all the aspects of the high jump technique.
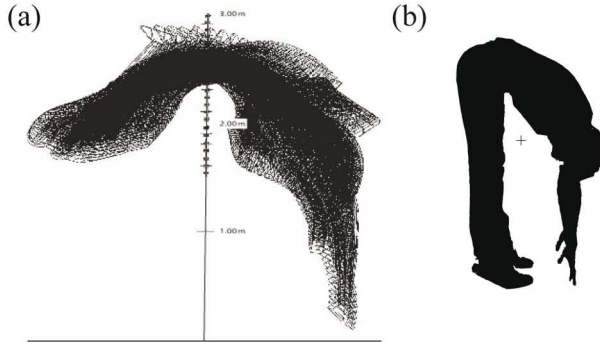
Figure 4: (a) Successive positions of the athlete's body during a high jump. The measured radius of curvature is $R_c = 0.95 \pm 0.1$ m. Data taken from [2]. (b) Optimal position for a pole vault attempt. The vertical segment is 40 cm long and the black cross shows the position of the center of mass of the jumper. The natural direction of curvature of the spine provides an increased absolute efficiency $\zeta \simeq 20$ cm.

3.2   Comparison with championship data

Our simplified modeling predicts an absolute efficiency ζ of a few centimeters for an athlete performing a perfect Fosbury-flop. We will now compare this prediction with the data obtained by J. Dapena for the five best jumps during 1992 Olympic Games (see table 2). All the five jumpers have cleared a bar standing at 2.34 m, but with quite different jumps. J. Sotomayor is the one with the lowest efficiency, as he had a peak height $h_{pk} = 2.46$ m (this didn't prevent him from winning the gold medal, as he was the only one to clear this bar on his first attempt!).

Athlete	h_{bar} (m)	h_{pk} (m)	h_{cl} (m)	ζ (m)
Conway	2.34	2.41	2.35	−0.06
Forsyth	2.34	2.44	2.39	−0.05
Partyka	2.34	2.39	2.36	−0.03
Sjöberg	2.34	2.33	2.35	0.02
Sotomayor	2.34	2.46	2.36	−0.10

Table 2: Performance of the 5 best high-jumpers during 1992 Olympics. h_{bar} is the height of the highest cleared bar for each athlete, h_{pk} is the peak height of the center of mass, h_{cl} is the clearance height for the jump and ζ the absolute efficiency of the jump. Data from [2].

On the other hand, the silver medal (P. Sjöberg) cleared the same bar, but he succeeded in keeping is center of mass lower than the bar during his entire jump, having an absolute efficency $\zeta = 2$ cm. All the other jumpers have a negative absolute

efficiency ζ. Nevertheless, we always find $\zeta \leqslant 10$ cm. This means that the all jumpers take advantage from the bending of their bodies: they jump over a bar that they would not be able to clear if they had a rigid body with a thickness $e = 20$ cm.

From this viewpoint, Fosbury flop (and to a further extend any jump technique involving a large curvature of the athlete's body) is an improvement with respect to other techniques in which the body remains straight. Physically speaking, the consequence of this bending is that the jumper is able to clear a potential bar having a lower potential energy. To some extend, this behavior can be related to a similar situation in physics where a particle can go through a potential barrier even if it has an energy lower than the barrier: quantum tunneling.

4 Quantum tunneling

Quantum tunneling belongs to a class of experiments of wave physics which present some unexpected non-classical behaviors. Tunneling occurs when a wave with a given energy is sent to a higher potential barrier, *i.e.* when there exists a region of space where this potential is larger than the wave energy. Contrary to the classical situation, it is nevertheless possible to observe a non-zero transmission of the wave through such a barrier. The origin of this phenomenon can be related to the evanescent nature of the wave inside the potential barrier. We will now briefly recall this physical situation in its simpler configuration, the unidimensional tunneling (more details can be found in [6]).

Let us consider a one-dimensional system made of a quantum particle (*e.g.* photon or electron). The state of this particle can be represented by its wave function $\psi(x, t)$. The dynamics of this particle obeys the Schrödinger equation. For stationary solutions, the wave function will obey:

$$\frac{d^2}{dx^2}\psi(x) + \frac{2m}{\hbar^2}\left(E - V(x)\right)\psi(x) = 0 \ , \tag{6}$$

with m and E the mass and energy of the particle, $\hbar$ the Planck constant and $V(x)$ an external potential depending only on the spatial coordinate x. We will look at the situation where the external potential has a rectangular shape, with a value V_0 in the central region (fig. 5(a)). We also impose that $E < V_0$. We can distinguish three regions, solve the Schrödinger equation in each of them, and match the solutions by continuity. Inside the barrier, the solution ψ_b is an evanescent wave (see fig. 5(b))

$$\psi_b(x) = A'_2\, e^{-\rho_2 x} \ , \tag{7}$$

with an exponential decay given by:

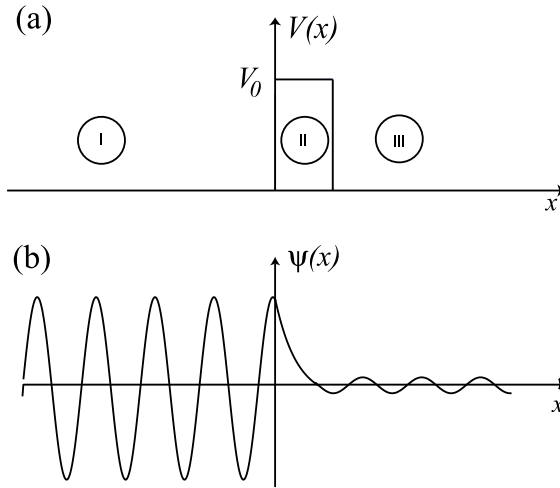$$\rho_2 = \sqrt{\frac{2m(V_0 - E)}{\hbar^2}} \ . \tag{8}$$

Figure 5: (a) Rectangular potential barrier, with $V = 0$ in the regions I and III, and $V = V_0$ in region II. The incident particle has an energy $E < V_0$. (b) Shape of the solution $\psi(x)$ for such a barrier.

The continuity of the wave ensures that there is a non-zero transmission through the barrier and we can compute the transmission coefficient T. For low probabilities, *i.e.* for $\rho_2 l \gg 1$ with l the width of the potential barrier, T has a simple expression:

$$T \simeq \frac{16E(V_0 - E)}{V_0^2}\, e^{-2\rho_2 a}\,. \tag{9}$$

Contrary to the classical prediction, a particle has a nonzero probability of getting through a potential barrier even if its energy is lower than this barrier: the wave function is is not equal to zero inside the barrier region, but is evanescent, following an exponential decay with a characteristic length $1/\rho_2$. For a barrier such as $a \leqslant 1/\rho_2$, there is a large probability for the particle getting through the barrier. This probability decreases when increasing the width of the barrier or decreasing the energy of the incident waves.

An important feature of quantum tunneling is the randomness of individual events. The calculation using wave functions only allows for a probabilistic description of this process. When the particle has an energy lower than the potential barrier, it has *some* probability to get across, but we are not able to predict the output of individual events.

This mechanism involving wave description of particles at microscopic scale has been able to describe successfully the alpha nuclear disintegration [7], and is used in standard analysis routines such as electron microscopy for example. It is commonly accepted that tunneling only occurs at microscopic scale, where quantum mechanics holds, and that it cannot be observed at larger scales. This is due to the fact that

classical mechanics use point-mass description to describe rigid systems, and do not allow for non-local objects. Nevertheless, it has been show that deformable bodies can present a form of tunneling, using a rope description [8] or a time-evolving distribution of point-like masses [9]. It has also been recently shown that walkers, that associate a bouncing droplet (the particle) and surface waves on a liquid bath at macroscopic scale, can present a form of tunneling [10]. This behavior was ascribed to the non-locality of the walkers, namely because of the spatial extension of their wave field which allow them to probe their environment. A convincing feature of this macroscopic tunneling was the randomness of single events, implying that the crossing probability was only defined for large statistics.

5   Discussion

Can we qualify high jump and pole vault as being a *classical case of tunneling*? We demonstrated that the jumper clears a bar with a lower potential energy than expected in classical mechanics. This appears in the data collected during 1992 Olympics, and we have shown that it can be related to the spatial extension and deformability of the athlete's body. His/her capacity to dynamically change the shape of the body allows him/her to clear a bar located a few centimeters higher than expected. From this point of view, the Fosbury-flop jumper and the pole vaulter are experiencing a form of classical tunneling.

On the other hand, this analogy has some clear limitations: the result of a jump is not random in the sense of quantum mechanics. Two identical jumps, with the exactly same Fosbury-flop by the athlete, will always give the same output. The random aspect in the jumps comes from the differences in the run-up, in the conversion of horizontal impulsion into vertical impulsion and in the efficiency of the body bending. This explains why the athlete are granted three attempts to clear a given bar. The reproducibility and efficiency of these phases are related to the athlete training, and cannot be ascribed to any physical process during the jump.

Finally, we never considered the energetic expenses of the athlete during the free flight. This can be estimated around several hundreds of joules (a human being can develop a peak power of a few kilowatts, and the free flight is typically lasting around one second), which is far larger than the energy difference between the peak heigh and the cleared heigh granted to the athlete using the Fosbury flop technique.

For all these reasons, we cannot say that the jumpers are tunneling through the bar they have to clear in the sense of *quantum tunneling*. Nevertheless, their jump has some common features with this phenomenon, and we should define this effect as a *classical case of tunneling*.

References

[1] J. Dapena. Mechanics of translation in the fosburyflop. *Med. Sci. Sports Exerc.*, 12(37–44), 1980.

[2] J. Dapena. *in Biomechanics in Sport.* Blackwell Science: Oxford., 2000, pp. 284–311.

[3] D. Thompson. *On Growth and Form.* Cambridge University Press, 1992 (1st ed. 1917).

[4] T.A. McMahon and J.T. Bonner. *On size and life.* Scientific American Library, New York, 1983.

[5] O. Helene and M.T. Yamashita. A unified model for the long and high jump. *Am. J. Phys.*, 73(10), 2005.

[6] Claude Cohen-Tannoudji, Bernard Diu, and Franck Laloë. *Mécanique Quantique.* Hermann, Paris, 1977.

[7] G. Gamow. Succesive alpha-transformations. *Nature*, 123(606), 1929.

[8] A. Cohn and M. Rabinowitz. Classical tunneling. *Int. J. of Theor. Phys.*, 29:215–223, 1990.

[9] A. Y. Davydov. Wave-particle duality in classical mechanics. *Proceedings of Emergent Quantum Mechanics conference - Vienna*, 2011.

[10] A. Eddi, E. Fort, F. Moisy, and Y. Couder. Unpredictable tunneling of a classical wave-particle association. *Phys. Rev. Lett.*, 102(240401), 2009.

Chapter V

Friction

1 Friction: an introduction, with emphasis on some implications in winter sports

by L. Bocquet
Institut Lumière Matière, Université Lyon 1 -
UMR CNRS5306, 69622 Villeurbanne

Abstract

Friction impacts many aspects of our daily life, and so does it in many sports. This introduction aims at giving an overview of the questions involved in friction, from its manifestation at our macroscopic scales, down to its fundamental origin at the micrometric and even nanometric scales. As a dedicated focus, we will put some emphasis on open questions in ski and ice friction and the role of waxing and capillary effects.

1 High Friction, Low friction

Walking in the streets on an icy day is not an enjoyable experience. One may loose grip to the ground at any time, with immediate and quite uncomfortable consequences. Along the same idea, for a cross-country runner, choosing inappropiate shoes on a rainy day with mud covering the trail can be dramatic for the performance. In both cases, this is of course because one needs to adhere on the ground in order to walk or run, so that the floor is able to sustain the backward force imposed by the walker.

One may multiply such examples from our everyday experience, showing how important is the role of friction in any aspect of life, nature and technology [1, 2]. Friction has certainly positive and negative aspects, if such an emotional statement has any sense from a physical point of view. In some cases, one may want to increase friction, as in in the above example, which can be extended to any situation involving gripping, *e.g.* gripping of tires, breaking, catching of objects, etc. In many other situations, one rather aims at *decreasing* friction. The goal of many technological applications is to reduce friction in order to diminish energetic losses and this has always been a great factor of progress. Going back to oldest ages, the invention of the wheel 3000 years before J.C. allowed to reduce considerably friction and resulted in a revolution for humanity. Still now, reducing friction is a motivating goal in technology: for example, more than 30% of the injected fuel energy in a car is still dissipated in friction losses, and this represents a huge amount of wasted energy [3].

Friction in sports

Back to the main topics of this article, tuning friction is a key motivation for improving performance in many sports. This is obviously the case of most winter sports, which involves gliding on a surface, snow or ice, in one way or the other: down-hill and cross-country skiiing, ice-skating, hockey (see the contribution by Haché below), curling, bobsleigh, etc., etc. In these differents cases, reducing friction is one of the main challenge. The case of classical (alternative) cross-country skiing is a bit peculiar, since it involves alternative periods of sliding and sticking. Accordingly, one wants to decrease forward friction (to slide), while increasing backward friction (to stick). In some ski models, this is achieved by asymmetric (saw-tooth) like patterns on the base of the ski, creating a kind of *friction diode.*

For other sports, a punctual increase of friction is useful: all racket sports, and specifically tennis or table tennis, make use of ball effects to distabilize the opponent, usually by giving the ball some spin during the collision with the racket. This requires sufficient friction to transform translational into rotational motion. In this book the contribution by Cohen *et al.* on squash reveals an even more subtle effect with a strange bounce of the ball in certain conditions, and taking its root in differential friction between different walls. This kind of effects is not restricted to these sports and for example bowling involves period of slip and no-slip rotation of the ball, for which the player has to deal with friction of the ball on the floor.

In a different context, increasing friction is sometimes welcome for very basic reasons: anyone who has played rugby on a rainy day knows how difficult it may be to grasp the ball when it is wetted by water. Also gymnasts and climbers use chalk to absord moisture from their hands, and improve grip. This points to a key aspect of friction between solid: sometimes it involves some fluid in between the surfaces at contact, which may drastically decrease the friction.

In the above discussion, I merely gave examples involving solid-on-solid friction.

But the domain of friction is actually far broader, and in order to be exhaustive, one should include also the questions of friction of solid moving in fluids, be it air, or water. This is for example highlighted in the chapter below on the physics of elastic spheres skipping on water by Helden *et al.*, where it is shown that deformation of objects may effectively reduce dissipation. These aspects are discussed in other parts of this book and I will leave them aside in the following discussion and focus on friction between solids. However, solid-on-solid friction often involve liquid lubricants, as examplified by the previous examples, and I anticipate that this will be a key aspect of friction in sports.

What does one need to know about friction?

Each sport has its own specificity, and each could be the object of a dedicated discussion. But it seems more appropriate here to provide some general ideas on the description of friction process from a physical perspective, and if possible, how this understanding may help improving performance for sports. At least identify what are the key ingredients on which one may play to tune the frictional behavior seems a reasonable goal to reach. Accordingly will give some hints about the origin of friction, rather than focusing on its macroscopic consequences. This understanding at smaller scales is somewhat subtle and involves many different fields of physics, from plasticity to capillarity. This is a complex but very rich domain.

Friction between solids has been the object of well documented books and reviews, for example the books by Bowden and Tabor [1] or the more recent overview by Persson [2]. Here I will recall the main ingredients and physical laws, and I will refer to these references for more specialized views.

2   Physics of Friction

A   The legacy of Amontons and Coulomb (and da Vinci)

In full generality, the notion of "friction" describes the dissipation that occurs whenever two surfaces glides against each other. It is intuitively associated to the notion of *grip*, or vice-versa of *slipperiness*. Friction is accordingly associated with dissipation: this is what stops the motion of objects. On a cold day, we usually rub our hands against each other to get some heat. In doing so, one has transformed the mechanical work into heat thanks to the friction between hands, and some energy has been lost in the process.

Most of phenomena associated to friction can be understood on the basis of the phenomenological laws of friction, which date back to the 18th century with the work of Amontons and Coulomb but first evidenced, like many other things, by Leonardo da Vinci 200 years before. These empirical laws introduce the notion of friction coefficient

as a key quantity. We will denote it as μ in the following; it is a dimensionless quantity, *i.e.* a number. The basic laws are expressed in the following simple way. Consider a object on a surface, *e.g.* a mass M on a table, with weight $F_N = Mg$ acting normal to the surface. One applies a tangential force F_T parallel to the surface. If the object is initially at rest, then motion will occur only for force F_T larger than a minimal force F_T^*, which is proportional to the normal force:

$$F_T^* = \mu_s \times |F_N| . \tag{1}$$

The coefficient μ_s is the static friction coefficient.

Now if the object moves at finite velocity on the surface, then the tangential force of friction is found experimentally to be proportional to the normal force:

$$|F_D| = \mu_d \times |F_N| . \tag{2}$$

The coefficient μ_d is the dynamic friction coefficient. In general μ_d is lower than μ_s.

The experiment show that for many situations involving *dry materials*, the dependence of μ_d on velocity V is weak: typically logarithmic, $\mu_d \propto \log V$, or a weak power law, $\mu_d \propto V^\alpha$, with a small exponent α. Also the static friction coefficient μ_s is found to depend on the "aging" time, *i.e.* the time t_w since the objects were put in contact. But again the dependence is relatively weak, varying typically as $\mu_s(t_w) \sim \mu_s^0 + B \log t_w$. In many situations with dry solid-solid contacts, one can forget about these weak dependences as a first guess to build an understanding. However for some aspects, these can play an essential role [2].

A key observation is that the coefficients μ_d and μ_s are found to be *independent of the contact area*, as was first reported by Leonardo da Vinci, see Fig. 1: whatever the surface of contact, the force to displace the object is always the same. We will come on this important point below, discussing its origin and consequences.
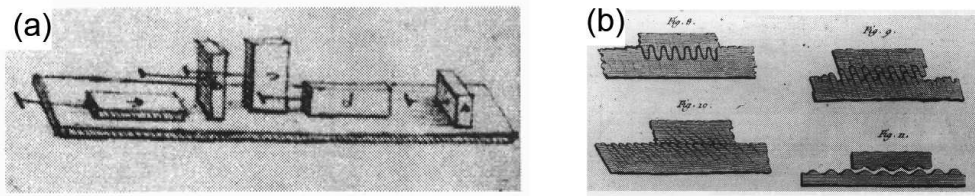

Figure 1: (a) Pictures from Leonardo da Vinci, illustrating his experiences showing that the friction coefficient does not depend on the contact area; (b) description proposed by Coulomb to account for friction. Pictures from ref. [4].

Values for the friction coefficient are typically of order $\mu \sim 0.3$ for many materials. But this is not a general rule and for example friction on ice has a very low friction coefficient $\mu \sim 0.01$, depending on the temperature [5].

Many phenomena, from the simplest to the most complex ones, can be interpreted at the level of these simple laws. Among others, one key consequence of μ_d being lower than μ_s is the phenomenon of stick-slip, whose implications span a variety of phenomena as diverse as the induced vibration of a violin cord under the motion of a bow, to earthquakes dynamics.

B   The physical origins: a few words

Beyond their subtle consequences, the simple nature of these laws also hides an incredible complexity. As we discuss now, their origins encompass processes that occurs at all possible length scales, from the macroscopic scale of the objects down to the molecular scale of the molecules. The fact is that many physical processes lead to Amontons-Coulomb type of law for the friction between sliding objects. Therefore these coefficients can have many origins, and it is difficult to disentangle the various mechanisms. Said differently, measuring a friction coefficient does not provide much information on the process at play.

The search for the origin of these friction laws has actually a long story, starting with da Vinci, and Coulomb and many others. In order to understand the origin of Amontons-Coulomb laws, there are two aspects to consider: (i) the origin of dissipation; (ii) the mystery behind the absence of surface dependence.

1 *Dissipation*

Dissipation has many possible origins. Friction is intuitively connected to corrugation and this has been the first explanation proposed by Coulomb, see Fig. 1-b. For such wavy surfaces, a simple argument allows to connect the friction coefficient to the typical slope of the material's corrugation, in the form $\mu \approx \tan \alpha$. However this argument assumes an intimate contact between the two contacting surfaces, which can only be achieved for *commensurate* surfaces: these are surfaces whose values of lateral periodicities are commensurate, *i.e.* their ratio is a rational number. Any disparity between the corrugation of the top and bottom surfaces will avoid an intimate contact and this leads to an essentially vanishing friction. One speaks of *incommensurate surfaces* in this case. This counter-intuitive prediction was confirmed very recently in experiments by Hirano *et al.* [6] and Dienwiebel *et al.* [7]: a vanishing friction is measured between surfaces with incommensurate atomic corrugations ! This is coined as "supra-friction".

This exceptional property, which is a kind of a graal for friction, is however only observed in drastic conditions, far from real life conditions: ultra-high vaccum, absence of contaminents, perfectly flat surfaces, etc. Actually it was shown that any intersticial contaminent which would be present between the two incommensurate contacting surfaces would lead back to finite friction [8]: these small particles take place in the interstices left between the surfaces, which in the end behave back as commensurate ones. And the presence of such contaminents can not be avoided: they

are either present in the atmosphere (dirt, oils, humidity,...) or produced by the friction process itselft, *e.g.* due to wear induced during sliding (think to the dirt left behind a chalk line). The presence of such intersticial matter is ususally coined as the "third body" in the tribology litterature (which is a bit of an euphemism to coin all uncontrolled material that may end between surfaces).

Note that the above arguments not explain why the dynamic friction coefficient is measured to be barely dependent on the sliding velocity. And this independence is not obvious by any means: the dynamics of matter usually obeys *linear response* and one would rather expect a *linear* dependence of the friction force on sliding velocity. This is what occurs for example for hydrodynamic friction. This independence suggests subtle dissipation process at the surface contacts, as well as non-equilibrium dynamics. It was actually suggested [9] that the zones of intimate contact between the two zones, which undergo very high pressures (as we will see below) may behave as a glassy materials. Such out-of-equilibrium materials exhibit yielding properties, in the sense that they flow above a finite force only [10]. This property is described in terms of a yield stress, σ_Y, which is the force per unit surface to bypass in order to make the material flow plastically. These questions are still a matter of intense work.

2 Surfaces

Another puzzling observation is the mystery of surfaces: whatever the surface in contact, as illustrated in Fig. 1, the friction force is identical. This very counter-intuitive behavior remained a mystery for more than 400 years and was given an explanation only in the 50's thanks to the work of Bowden and Tabor [1]. As shown by these pioneers of modern tribology, the key to understand friction is that the real contact between surfaces is very sparse due the *roughness of interfaces*. The real area of contact, $\mathcal{A}_{\text{real}}$, is much smaller than the apparent one $\mathcal{A}_{\text{app}}$, as one would naively expect from an eye inspection. Several works could verify this property by direct vizualisation of the true contact [2]. This observation show that an object resposing on surface makes only very few contacts with the underlying surface. The picture is that of a very diluted contact area, made of contact spots a few micron squared in size, see Fig. 2. Typically the ratio $\mathcal{A}_{\text{real}}/\mathcal{A}_{\text{app}}$ can be as low as 0.1%, $\mathcal{A}_{\text{real}}/\mathcal{A}_{\text{app}} \sim 0.001$.

An immediate consequence is that the normal force F_N pushing the object towards the surface is distributed only through a small number of contact (typically with micron size) and the local pressure acting on these contacts, $P_{\text{contact}} = F_N/\mathcal{A}_{\text{real}}$, is expected to be huge. In such conditions, the material enters a *plastic* regime in which the material deforms under a fixed pressure $P_{\text{lim}} = H$, with H the so-called hardness of the material. Accordingly the real contact area is given as $\mathcal{A}_{\text{real}} = F_N/H$. Now, a second consequence associated with plasticity of contacts is that the lateral friction force per unit surface on a contact – the shear stress –, is expected to be also a material constant, which we will denote σ_Y. Altogether, we thus expect $F_T = \sigma_Y \times \mathcal{A}_{\text{real}}$.
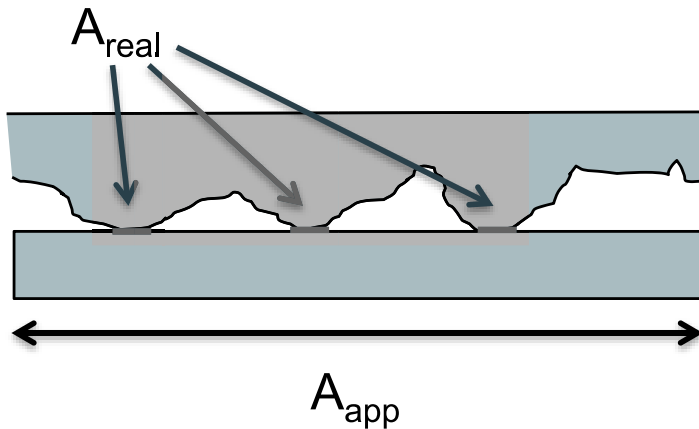
Figure 2: Sketch of a contact between two rough surfaces in contact. The real contact area $\mathcal{A}_{\mathrm{real}}$ is much smaller than the apparent one $\mathcal{A}_{\mathrm{app}}$.

Finally one obtains the friction coefficient $\mu = F_T/F_N$ as:

$$\mu = \frac{\sigma_Y}{H} \; . \tag{3}$$

The friction coefficient is thus the ratio of two material properties, the shear stress and the hardness, and is accordingly independent of the apparent area of the object.

Some recent investigations have explored more specifically the plastic nature of the contacts [11], showing that they behaved like a glassy material, as we quoted earlier. The deformation properties of glassy materials are still the object of intense work. These materials raise considerable fundamental difficulties, as they exhibit properties intermediate between that of a liquid and a solid, with the existence of yield stress. The glassy materials are out-of-equilibrium systems, exhibiting for example *aging* of their properties, which are observed to evolve over very long time scales, or non-newtonian behavior under flow, with a weak velocity dependence of the shear stress under flow. These behaviors do echo those observed for the solid friction coefficients. For example aging of the static friction coefficient is usually attributed to thermally activated creep of the nanometric contacts between solids.

Altogether, this very sparse nature of the contact is a key to understand friction properties. One cannot consider that the contact between objects is intimate, but ocurs only through a small number of contact points.

3 Capillarity and humidity effects

The wetting properties of surfaces also affect the friction properties in several aspects. Humidity does affect friction and an increased friction is measured in more humid environment [2, 12–14]. The aging property of friction, *i.e.* the logarithmic

dependence of the friction coefficient on the time of stationary contact, is also found to depend on humidity for stones, paper, glass surfaces, as well as for granular materials; but not for hydrophobic materials as teflon [2]. The origin of this phenomenon is the formation of liquid bridges between the two surfaces at contact (in the region of real contacts), by capillary condensation of the water vapor into its liquid phase. For wetting situations the liquid bridge is at a negative pressure, typically $\Delta P \sim \gamma_{LV}/\ell_R$, with γ_{LV} the liquid vapor surface tension and ℓ_R a typical nanometric scale (the Kelvin radius, which is fixed by humidity due to thermodynamic equilibrium [13]). This leads to huge pressure in the capillary bridges, up to values of order $\Delta P \sim 700$ atm (for a 1nm Kelvin radius to fix ideas). This pressure drop leads to an increased normal adhesion force, f_{adh}, which adds up to the normal load: this increases the real area of contact and thus friction. Typically this mechanism leads to an humidity induced ageing of the friction coefficient which behaves as

$$\mu(t_w) = \mu_0 + \frac{A}{\log(RH^{-1})} \times \log(t_w) \tag{4}$$

with A some material constant. For hydrophobic materials, condensation of capillary bridges does not occur as it is thermodynamically unfavored, and this aging contribution disappears.

C   Lubrication

Up to now we have focused our discussion on dry contacts, in which the two sliding surfaces are in direct contact. However low friction usually involves lubrication by a fluid located in between the two objects.

The fact that fluid may lead to low friction is known for thousand of years [4]. It is intuitively expected that replacing direct solid-on-solid contact by solid-liquid contact will reduce considerably the friction force. Still, lubrication can be sutble, as highlighted by a simple example: it is a common experience that hands wetted by oil slips much more than hands wetted by water, although the viscosity of water is much lower than the viscosity of oil. At the origin of this counter-intuitive behavior is the properties of the intersticial liquid film. By flowing less easily, the more viscous liquid maintains an intersticial liquid film, thereby avoiding direct solid-solid contact. This is the main role of the lubricant. Lubrication usually involves highly viscous oils, but water or even gases can lubricate contacts and reduce accordingly the friction. Going more into the details of lubrication, let us consider a fluid film with thickness h_0 and viscosity η confined between two surfaces. For a lubricating film h_0 much smaller than lateral size of the object, then the fluid inertia is negligeable and the friction shear force is typically

$$F_T \sim \mathcal{A} \eta \frac{U}{h_0} \tag{5}$$

with $\mathcal{A}$ the lateral (wetted) area of the object. For a fixed film thickness h_0, the friction force is therefore linear on velocity U, and so does the friction coefficient.

Now in many situations, the thickness h_0 is not fixed *a priori*, but the normal force on the object is imposed. In this case h_0 results from a mechanical equilibrium itself: the flow of liquid is able to create an excess pressure, which levitates the object above the surface. To fix ideas, consider an object with lateral size L, sliding at velocity U on a surface. A film of liquid separates the object from the surface. The excess pressure can be estimated from the stationary (Navier-)Stokes equation:

$$0 = -\vec{\nabla}P + \eta\Delta\vec{v} \tag{6}$$

(Δ the laplacian, and $\vec{\nabla}$ the gradient). For this film $h_0 \ll L$, the velocity is sheared over the small thickness h_0 of the film, while the pressure drop is built over the lateral size L of the object. One obtains therefore the excess pressure $\delta P = P - P_0$ (over the equilibrium value) as

$$\frac{\delta P}{L} \sim \eta\frac{U}{h_0^2} \ . \tag{7}$$

The lift force sustaining the object is therefore of order

$$F_N \sim \mathcal{A} \times \delta P \sim \mathcal{A}\eta\frac{LU}{h_0^2} \tag{8}$$

with $\mathcal{A}$ the lateral area of the object. If the normal force is fixed, *e.g.* by the weight of the material $F_N = Mg$, then the film thickness is obtained as

$$h_0 \sim \sqrt{\frac{\mathcal{A}\eta UL}{Mg}} \ . \tag{9}$$

Gathering results from Eqs. (5-9) the friction coefficient $\mu = F_T/F_N$ then scales as

$$\mu \sim \frac{h_0}{L} \sim \sqrt{\frac{\eta U\mathcal{A}}{MgL}} \propto U^{1/2} \ . \tag{10}$$

As $h_0 \ll L$, one thus expects μ to be small. It is predicted to exhibit a non-linear square-root dependence on velocity U.

I deliberately stayed at a scaling level to discuss this phenomenon. A more complete analysis of lubrication can be found in many textbooks, for example in Ref. [2]. I would like to emphasize however that this scaling analysis hides some important subtleties behind lubrication. If the object is completely back-to-front symmetric, then it may be demonstrated from Stokes equation that the lift force is exactly vanishing. This results from the time-reversal symmetry of the Stokes equation. Said differently, the shear flow created between two parallel walls does not create an excess pressure

and thus cannot levitate the object. But if the surface of the top object is inclined with an angle α w.r.t. the bottom surface, then the lift force can be calculated (for small angles α) as

$$F_N \sim \alpha \times \mathcal{A}\,\eta\,\frac{LU}{h_0^2} \tag{11}$$

showing that it vanishes for $\alpha \to 0$ as expected. Only for finite angle α is the lubrication able to levitate the object. A coupling to the orientational degrees of freedom should therefore be involved for a complete description. We shall come back to this below.

3   Sliding on ice and snow: reactive lubrication

The friction coefficient of most materials on ice and snow are usually extremely small, with values typically as low as $\mu \sim 0.01 - 0.03$ depending on the conditions [5, 15–17]. This is at least one order of magnitude smaller than what is observed with dry friction involving other materials (typically $\mu \sim 0.3$ as quoted above). This specificity is definitely *the* reason why winter sports are flourishing: just imagine for one second cross-country ski race on sand, or a curling competition on a macadamized surface, this is just impossible.

Such low values of friction coefficients are an exception in tribology and this suggest that sliding on these frozen materials necessarily involves some lubrication of the contacts by fluids in one way or the other. This was first suggested in the 30's by Bowden and Hughes following their work on ski friction [15]. It is now accepted that friction on snow and ice involves sliding on a liquid film. But the origin of this film, as well as the mechanisms controlling its thickness, remains a complex matter with many open questions which are still debated today [5].

From a physics perspective, a very interesting aspect is that under sliding, the lubricating liquid results from the melting of the frozen water itself (with various potential mechanisms at play, as we discuss below). The amount of liquid in the contact is therefore not fixed *a priori*, but results frome the sliding process itself. In some sense, this bears some analogy to the famous Leidenfrost effect [18], whereby a drop of water is able to levitate on a hot surface, thanks to the flow induced by the phase transformation of liquid water to vapor.

We give below some very basic accounts of the vast litterature concerning ice and snow friction and give a few examples related to sports. We will also insist on the open questions and future challenges in this field.

A   Ice friction

1   Some basics

Many sports involve sliding on ice: skating, curling, bobsleigh, ice hockey (as discussed in the following chapter by Haché).

The friction properties of ice are exceptional in various aspects: not only the friction coefficient is low, typically $\mu \sim 0.01$, but even more, it takes small values even in the quasistatic regime of very slow sliding, making ice so slippery (this of course depends on the temperature). The mechanisms behind this exceptional behavior still remain debated [5, 19], but there are a number of experimental evidences showing that the top surface of ice is melted. This idea was actually first proposed by M. Faraday ... already in 1859 [9] ! After some detours putting forward the pressure melting of ice – an idea now discarded –, experiments (using various research tools like Atomic Force Microscopy or X-ray scattering,...) seem to confirm the surface melting mechanism. This points to a liquid-like film existing at the top surface of ice in contact with air, with an equilibrium thickness of the film which depends on temperature, but was measured typically in the range $10^0 - 10^2$ nanometers. Some quite large discrepancy however exists between measurements using different techniques.

The presence of this film is usually invoked to explain why ice is slippery, even without sliding: this film – even nanometric – lubricate the contact and the friction force would be expected to become vanishingly small as the sliding speed decays to zero, in line with Eq. (5). This is of course only true if this melting film exhibits properties of real liquids, which is not obvious. Also one may however raise the question of the existence of such a film when the ice is in contact with a solid surface. This question is still open.

Now, under finite sliding velocity, the friction results from the interplay of various mechanisms. This is evidenced experimentally by the rather complex behavior of the friction coefficient versus temperature and velocity. Basically, the friction is high at low temperature, say between -20 – -10°C, then decreases towards a minimum (low) value in a temperature range around 0°C and then increase again for positive temperatures [5, 15]. This behavior is attributed to the various degrees of lubrication which might occur for different temperatures: low lubrication at low temperature, increasing lubrication around the melting temperature $T \sim 0$°C, and thick lubrication films in warm conditions. The increasing friction in this latter regime is then attributed to a so-called "capillary suction" effect, on which we will come back below. The dependence on velocity may be split roughly in two different regimes [5, 20, 21]:

- for low temperatures, various experiments show consistently that the friction coefficient *decays* with velocity as $\mu \sim U^{-1/2}$;

- for larger temperature, it *increases* with temperature as $\mu \sim U^{\alpha}$, with $\alpha \approx$

0.5 − 1, depending on materials and experiments.

We note that experimentally measurements at low temperature appears to be more reproducible and consistent for various sliding materials, as compared to friction measured at larger temperature, for which experimental data are much more spread and strongly material dependent.

Modelling these various behaviors remains a challenge, and the underlying processes are amazingly complex and entangled. But several attempts to capture the basic underlying mechanisms of ice friction have been proposed. The main idea, in line with the seminal work of Bowden and Hughes [1], is that the heating produced by the friction process is able to melt further the ice in the contact and increase the thickness of the lubrication liquid water film [16].

Following Colbeck [16], the basic (elementary) picture is that of a slider moving on an ice grain, with size r, with a lubrication film of thickness h separating the grain from the slider (see a sketch in Fig. 3-Left). The basic description consists in balancing the viscous heating produced by the flow with the energy associated with melting and heat loss. Forgetting about geometrical prefactors, this balance is written typically as

$$r^2 \, h \times \eta \left(\frac{U}{h} \right)^2 \approx L_w \times r \, h \, U + \kappa \, r^2 \frac{\delta T_0}{\sqrt{\frac{\kappa}{\rho c_w} \times \frac{r}{U}}} \; . \tag{12}$$

Let us discuss the various terms in this equation. The left term correspond to the viscous heating produced by shearing the liquid film. The first term in the right-hand side correspond to the power associated with the transformation of ice into liquid, with L_w the latent heat of water (per unit volume), and the second term in the right-hand correspond to the heat conduction into ice and slider; κ, ρ, c are an effective thermal conductivity, density and heat capacity of the interface with excess temperature δT_0. The latter term corresponds to the heat flux dissipated by thermal diffusion over the time-scale of the contact $t \sim r/U$.

For small films, which would correspond to low temperatures, the second term in the r.h.s. is predominant and one deduces that the film thickness scales as $h \propto U^{3/2}$. The resulting friction force, as obtained from Eq. (5), or equivalently the friction coefficient, thus scales as

$$\mu \propto F_T \approx r^2 \eta \frac{U}{h} \propto \frac{1}{\sqrt{U}} \; . \tag{13}$$

For larger films, one would rather balance the l.h.s. of Eq. (12) with the first term in the r.h.s., yielding $h \sim \sqrt{\eta \, rU/L_w}$ and the friction coefficient scales as

$$\mu \propto \sqrt{U} \; . \tag{14}$$

These predictions for the velocity dependences reproduce, at least qualitatively, the experimental observations for friction in both cold and warm temperatures regimes.

However this relative success should not hide the fact that the arguments above suffer from many uncontrolled assumptions and shortenings. They constitute an idealized view, which lacks of strong experimental support. The contact between the ice and the slider is most probably mixed, with both lubricated regions and direct solid-solid contacts and a full description should take this composite nature into account. Experiments at the scale of a single micrometric contact are accordingly lacking. Indeed, while a measurement of the melted water film thickness under sliding has been reported by Ambach and Mayr [16], a full exploration is necessary to disentangle the various effects at play. Further measurements of the water film would be needed, in order to explore its variations versus velocity and temperature. Also the lateral spatial extension of the film could be a key factor on which information is lacking.

Finally the nature of the slider surface (hydrophilic versus hydrophobic) should be considered, as this was shown to have some important impact on the friction for temperature around melting, as shown by Kietzig *et al.* [5]. The fact that most ski base are hydrophobic, as well as waxes, is a point which desserves more investigations. We will come back on this point below when discussing snow friction.

2 An illustrative example: curling

Curling, which is an icy version of pétanque, is an interesting example of a sport where friction plays a crucial role, sometimes in some unexpected way. Players slide some big stones ("rocks") on an ice surface towards a target. The trajectory of the stone can be affected by two players who can modify the ice in front of the stone by sweeping it vigoroulsy with brushes. The ice temperature is typically around $-4°C$ and the ice surface is pebbled by spraying water droplets, making it quite rough. The length and trajectory of the path is then affected by the sweeping of the ice: by reducing the friction, sweeping more leads to longer and straighter trajectories.

An interesting effect concerns the curl of the stone. By inducing a slow spin, the trajectory is observed to curve in the same direction as the imposed rotation: rotating clockwise leads to a bending towards the right. This seems intuitive ... but goes actually against expectations made on the basis of Coulomb laws only [22], which would predict a bending in the other direction (due to the fact that the friction force at the front of the decelerating stone is larger than the friction force at its back, leading to a bending against the rotation). And experiments done with a rotating glass on a table do actually confirm this view. This means that ice is very special in this process and the specificities of ice friction should enter the game. The key question is then to understand why the friction at the front of the stone is *smaller* than at its back. As reported by Courty and Kierlik [22], this puzzling questions has generated a strong debate between two authors, M. Shegelski [23] and M. Denny [24], who both have an interpretation for this anti-rotation bending. Denny suggests that

debris accumulate at the front, thereby smoothening the front part of the stone-ice contact and decreases the friction accordingly. On the other hand, Shegelski invokes wet friction, arguing that the lubricating liquid film is thicker at the front than at its back, thereby decreasing friction ahead. Solving the debate certainly require to look more closely at the stone-ice contact.

But this funny behavior points in any case to the specific behavior of ice as compared to any other surface.

3   Beyond liquid friction: the impact of air lubrication on the sliding motion of the hockey puck

We consider here a second situation occuring in ice hockey: the fast motion of the hockey puck, which can reach velocities as high as 180 km/h, *i.e.* 50 m/s!

At such high velocities and for the typical temperature of a skating ring typically around -10 – $-5°$C, the friction coefficient on ice is expected to be extremely small. But still, we raise an academic question: does the puck touch the ice, or not?

For the air-hockey game, the puck is indeed levitated by an air flow blowing out of the table, which allows to reduce considerably the friction on the table. But in real ice hockey, can the air levitate the puck? The question is useless . . . but worth answering as an exercise. And ice hockey is claimed to be the fastest existing collective sport, and the low friction on the ground is a key factor to maintain a maximum speed of the puck.

Actually we can start with an observation, not on ice, but on a bar counter: if one throw vigorously a coin on this very flat surface, one may see sometimes the coin going fast and travel a long distance, as if the friction coefficient was very small. Such low friction suggests lubrication and air is the only fluid around in this case.

Can air levitate a sliding object, even though the viscosity of air is very small? It can indeed, as one may verify immediately from the lubrication theory that we developped above. The air viscosity is typically $\eta_{\mathrm{air}} = 1.8\,10^{-5}Pa.s$, *i.e.* two orders of magnitude smaller than water. Using Eq. (8-9), with the characteristics of a hockey puck (diameter $D \sim 8$ cm, $M = 170$ g), with a velocity $U \sim 25$ m/s, one gets for the air thickness $h_0 \sim 300\mu$m and this corresponds to a friction coefficient $\mu \sim h_0/D \sim 0.04$ which is indeed very low.

Following a remark that we made above, a full description would require to take into account the angle, say α, made by the hockey puck with respect to the ground surface. This angle is not fixed a priori, and we have therefore two unknowns in this problem: α and h_0. A supplementary equation is therefore required, which can be obtained by writing the balance of torques acting on the hockey puck. We leave this (rather academic) problem as an exercize to the reader. We only mention that the angle α is obtained as a (weak) function of the puck aspect ratio e/D (with e the

thickness of the puck), and independent of the velocity, so that the previous scalings of h_0 with U are maintained.

Altogether, it may well be that hockey puck do not touch the ground. A closer look would be necessary to answer this question, which we leave for future work.

B   Sliding on snow and some open questions

1   From ice to snow friction

Snow is an even more complex material as compared to ice: snow conditions are multiple, from cold to wet, with a variety of grains shapes, from hard facetted crystals to wet grains; snow is also a multiscale material, made of an assembly of small ice crystals or grains. It has usually a small resistance to plough, associated with a small hardness at large scale ($H_{snow} \sim 50$ kPa, with of course large variations depending on the snow conditions), while the hardness of ice is several orders of magnitude higher ($H_{ice} \sim 10$ MPa). This implies that the contact between the ski and snow is usually quite good, with a real contact area which is an appreciable fraction of the apparent one [21]. This is in contrast to the case of usual solid-on-solid contact that we discussed above. However note that, at the scale of the ice grains, the contact area can be much smaller, due to the high hardness of the ice.

In the end, a lot of properties observed in snow friction results from the contact of the ice crystals with the slider and the discussion above on ice friction is relevant for snow as well: this involves small friction coefficients, with various regimes depending on temperature, as well as the notion of reactive lubrication induced by heating [16]. Further contibutions are however the plowing of snow in front of the ski and snow compaction below the ski, which we leave aside here.

2   Snow friction and capillarity

One aspect of ski friction which remains essentially an open question is the contribution of capillarity. Several observations concur to state that capillarity has probably a major effect on snow friction: while snow and ice friction are low for temperature below melting, the friction coefficient increases again for temperatures above around melting and in wet conditions, in spite of the fact that lubrication is expected to be most effective there with thick liquid films; ski surface are usually hydrophobic, and PTFE was introduced as a material for the base to minimize friction [1]; waxing consists in adding a hydrophobic coating on the ski base in order to reduce the friction coefficient.

A capillary suction mechanism sets up, which increases friction [16]. Several hypothesis were put forward: an increase of the contact area, or an increase of drag due to breaking of capillary attachements. However there is a real lack of understanding of these behaviors up to now and physical mechanisms relating surface wetting to

friction are clearly missing. Here we propose some leads, which would desserve closer experimental look in the future.

Capillary suction in mixed friction – Let us consider a situation with a temperature close to melting, $T \sim 0°$C. In the picture proposed by Colbeck for the lubricated film, see Fig. 3-Left, the wetting properties are not considered and the shape of the film is drawn quite arbitrarily. However, the water bridge should connect the surface by obeying the Young's law on the surfaces, with a contact angle fixed by thermodynamics at the surface. While the ice is probably wetting for the liquid water (thus a vanishing contact angle), one should consider the presence of a finite contact θ between the water bridge and the base of the slider, see Fig. 3-Right. For a hydrophilic surface, as in Fig. 3-Right, $\theta < 90°$, while for hydrophobic surfaces one would have $\theta > 90°$. PTFE coating (teflon) gives a contact angle $\theta \approx 120°$ for water.
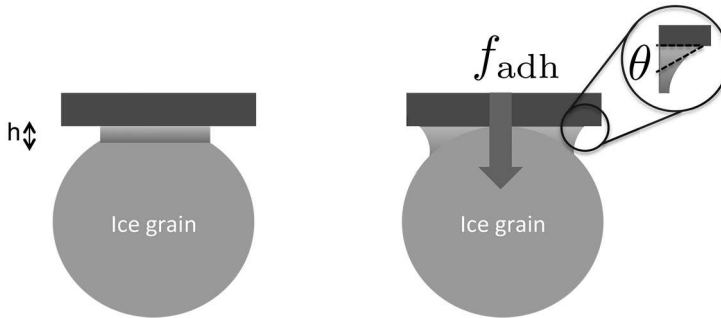

Figure 3: Ice grains in contact with a slider: sketch for the water film and influence of the wetting properties.

For a hydrophilic surface, the liquid meniscus is therefore bent toward the interior of the liquid, and a negative pressure drop builds up in the liquid bridge. This leads to an adhesive force between the slider and the ice grain, which will in the end increase friction. Similar phenomena occurs in solid-on-solid friction and in granular materials, as we discussed above [13, 25].

For a single spherical ice grain this adhesive force may be calculated as

$$f_{\text{adh}} = 2\pi\gamma_{LV}\, r\,(1 + \cos\theta) \tag{15}$$

where γ_{LV} is the water-vapor surface tension ($\gamma_{LV} \simeq 72$ mJ/m^2) and r the grain radius. This force is to be compared with the normal force acting on one grains due to the weight of the skier, $f_N = Mg/n_g$, where n_g is the number of grains in contact. The latter is $n_g = \mathcal{A}_{\text{real}}/\pi r^2 \sim \phi\,\mathcal{A}_{\text{app}}/\pi r^2$ (with $\phi = \mathcal{A}_{\text{real}}/\mathcal{A}_{\text{app}}$ the fraction of area in real contact, which is relatively large for snow due to its small hardness). Using $\mathcal{A}_{\text{app}} = 0.3$ m^2, $\phi \sim 0.4$, and $r = 50\mu$m (to fix ideas), one gets a rough estimate for the normal force per unit grain in contact $f_N \sim 7.10^{-5}$N, to be compared to the

adhesion force $f_{\text{adh}} \sim 5.10^{-5}$N (estimated with $\theta = 0$). This shows that capillary adhesion forces constitute a non negligeable part w.r.t. the weight. Going back to the definition of a friction coefficient μ between the ice grain and the slider, the friction force is proportional to the total normal force acting on the grain, which is now the sum of the two previous forces: the weight and the capillary adhesion force, so that the effective friction coefficient writes $\mu_{\text{eff}} = \mu \times (1 + f_{\text{adh}}/f_N)$ and using previous expressions one gets

$$\mu_{\text{eff}} = \mu \times \left[1 + \frac{2\pi\gamma_{LV}rn_g}{F_N}(1 + \cos\theta)\right] \ . \tag{16}$$

In practice this previous estimate does not account for the hydrodynamic dissipation occuring insider the water film. This takes a typical value $f_{\text{hyd}} \sim \eta_w \mathcal{A}_{\text{water}} \times U/h_w$ with h_w the typical thickness of the water film. For a spherical geometry, $\mathcal{A}_{\text{water}} \sim h_w \times r$ and $f_{\text{hyd}} \sim \eta_w rU$. Altogether one predicts

$$\mu_{\text{eff}} = \mu \times \left[1 + \frac{2\pi\gamma_{LV}rn_g}{F_N}(1 + \cos\theta)\right] + \frac{\eta_w rn_g}{F_N}U \ . \tag{17}$$

Such an expression is compatible with the experimental findings of Bauerle for friction of polyethylene on ice, close to melting [21].

It emphasizes the role of hydrophobicity, through the contact angle θ of water on the ski base material. A large contact angle $\theta \to 180°$ decreases capillary adhesion and thus the friction coefficient. This would suggest to use *superhydrophobic* surface with $\theta \approx 180°$ as a ski base, in line with the attempts of Kietzig *et al.* [5]. These materials are however usually fragile and could not resist the mechanical constraints associated with high speed skiing.

The above description is a first attempt to include capillarity effects and again, some more experimental insight on the wetted area are needed in order to build a proper model.

Some open questions – As last remarks, let us finish this discussion of snow friction by open questions. And there are many. First, for very wet conditions, a "suction" of water from the ground is usually described by skiers. This leads to an increase of friction. While we will not explore this phenomenon in detail, one may propose some hints to understand it. One remark is that due to partial wetting, a negative capillary pressure builds up in the liquid close to the ski, typically $\Delta P \sim \gamma_{LV}(1 + \cos\theta)/\ell_R$b with ℓ_R the radius of curvature of the bridges, typically $\ell_R \sim r$ the grain size (in the regime of very wet conditions). This pressure drop will induce an inward water flow from the wet snow, which acts therefore as capillary suction. The mass of water transported by this process leads to an increased dissipation for the skier, and thus an increased friction coefficient. It would be interesting to explore further this process experimentally.

Another remark concerns the stability of capillary bridges connecting the snow to

the ski base. In contrast to the picture given *e.g.* in Fig. 3, these capillary bridges are *dynamic* by nature: the snow grains are fixed to the ground and the ski base slides at a finite velocity U. This situation is very close to the forced wetting situation. In a very different context, a similar situation occurs for the impact of spheres in a bath of water [26]. It is accordingly expected that the contact line may be distabilized for large relative velocities of the contact line versus the slider. A threshold velocity U^* is measured above which the contact line disappears, with U^* of the order of a few meters per second. Also U^* is found to be a function of the contact angle itself: it decreases for hydrophobic surfaces, behaving as $U^* \propto (1 + \cos\theta)^3$ for $\theta > 90°$, in agreement with theoretical predictions [26]. While the connection to the capillary effect remains to be properly explored in the context of wet snow friction, this mechanism is anyway expected to play a role in the stability of the capillary bridges connecting the ski to the snow, as well as their lateral extension and dispersion. Some experimental exploration is required here also.

4   Conclusions

Friction is a fascinating problem where many domains of physics can meet: material properties, elasticity, plasticity, capillarity, thermal transport, hydrodynamics, phase transitions,.... While it is simple to measure a friction coefficient, friction results from a complex interplay of many phenomena occuring at many scales, from macroscopic down to nano- scales.

Altogether the discussions in this chapter raise more questions than they provide answers. In particular there are still a lot of mysteries behind the friction on ice and snow. Meaning that there are still unexpected ways to tune and control it ... and thus improve performance in sports involving sliding on ice and snow.

Though important for practical purposes, the friction coefficient does not provide much insights into the mechanisms at play. A friction coefficient is a combination of many factors which are difficult to disentangle. There is accordingly a strong need for new experimental investigations at smaller scales, in particular at the scale of the underlying lubrication film, as well as the scale of the ice/snow grain, and the scale of capillary bridges. This is crucial to get some more information on how wetting and hydrophobicity couples to high velocity water flows. Obtaining some functional dependence of the water film, as well as its extension and shape, as a function of these factors is a crucial step to propose a proper understanding of friction on ice and snow.

From a more fundamental point of view, modern modelisation tools would be extremely useful in providing a new point of view in the field. For example, phase field models, incorporating phase transformation into the (hydro)dynamics [28, 29], could be able to describe the subtle couplings associated with the reactive hydro-capillary mechanisms described above.

Snow and ice friction are example of reactive friction and can thus be considered to belong to Leidenfrost type of phenomena, whereby phase transformation is at the source of the specific dynamics of the system. This perspective might be inspiring for further developments.

Acknowledgements

References

[1] F.P. Bowden and D. Tabor, *The friction and lubrication of solids* (Clarendon press, London, 1950).

[2] B.N.J. Persson, *Sliding friction, physical principles and applications* (Springer, Berlin, second edition).

[3] S. Chu and A. Majumdar, "Opportunities and challenges for a sustainable energy future" *Nature* **488** 294 (2012).

[4] D. Dowson, *History of tribology* (Longman, New York, 1979).

[5] A.-M. Kietzig, S.G. Hatzikriakos and P. Englezos, "Physics of ice friction", *Journal of Applied Physics* **107**, 081101 (2010).

[6] M. Hirano, K. Shinjo, R. Kaneko and Y. Murata, "Observation of superlubricity by scanning tunneling microscopy", *Physical Review Letters*, 78, pp.1448-1451 (1997).

[7] M. Dienwiebel *et al.*, "Superlubricity of Graphite", *Physical Review Letters*, 92, 126101 (2004).

[8] G. He, M. Müser, M. Robbins, "Adsorbed Layer and the origin of static friction", *Science* 284 1650 (1999).

[9] T. Baumberger and C. Caroli, "Solid friction from stickslip down to pinning and aging", *Advances in Physics* **55**, 279 (2006).

[10] R.G. Larson, "The Structure and Rheology of Complex Fluids" (Oxford University Press, Oxford). -

[11] L. Bureau, T. Baumberger, C. Caroli, "Jamming creep at a frictional interface", *Physical Review E*, 64, 031502 (2001).

[12] J. Crassous, L. Bocquet, S. Ciliberto and C. Laroche, "Humidity effect on static aging of dry friction" *Euro-physics Letters* **47** 562 (1999).

[13] L. Bocquet, E. Charlaix, S. Ciliberto, J. Crassous, "Moisture-induced ageing in granular media and the kinetics of capillary condensation" *Nature* **396** 735 (1998).

[14] E. Riedo, F. Levy and H.Brune, "Kinetics of Capillary Condensation in Nanoscopic Sliding Friction" *Physical Review Letters* **88** 185505 (2002).

[15] F.P. Bowden and T.P. Hughes, "The mechanism of sliding on ice and snow", *Proc. R. Soc. London, Ser. A*, **172**, 280 (1939).

[16] S.C. Colbeck, "The kinetic friction of snow", *Journal of Glaciology*, **34**, 78 (1988).

[17] F.P. Bowden, "Friction on snow and ice and the development of some fast-running skis", *Nature* **176**, 946 (1955)

[18] A.-L. Biance, C. Clanet, D. Quere, "Leidenfrost drops", *Physics of fluids* **15**, 1632 (2003).

[19] R. Rosenberg, "Why Is Ice Slippery?", *Physics Today*, 50, December 2005.

[20] L. Baürle, D. Szabò, M. Fauve, H. Rhyner and N.D. Spencer, "Sliding friction of polyethylene on ice: tribometer measurements" *Tribology Letters*, **24**, 77 (2006).

[21] L. Baürle, "Sliding Friction of Polyethylene on Snow and Ice", Dissertation ETH Nr. 16517 (2006).

[22] E. Kierlik and J.-M. Courty, "Pierre qui tourne n'amasse que doute", *Pour la Science* **388** (2010).

[23] E.T. Jensen and M.R.A. Shegelski, "The motion of curling rocks: experimental investigation and semiphenomenological description", *Canadian Journal of Physics* **82**, 791 (2004).

[24] M. Denny, "Curling rock dynamics: towards a realistic model", *Canadian Journal of Physics* **80**, 1005 (2002).

[25] L. Bocquet, E. Charlaix, F. Restagno, "Physics of humid granular media", Comptes Rendus de Physique **3** 207 (2002).

[26] C. Duez, C. Ybert, C. Clanet, L. Bocquet, "Making a splash with water repellency", *Nature Physics* **3** 180 (2007).

[27] D.M. Anderson, G.B. McFadden, A.A. Wheeler, "Diffuse-interface methods in fluid mechanics", Annual Review of Fluid Mechanics **30** 139 (1998).

[28] I. Steinbach, "Phase-field models in materials science", Modelling and Simulation in materials science and engineering **17**, 073001 (2009).

[29] T.U. Kaempfer, M. Plapp, "Phase-field modeling of dry snow metamorphism", *Physical Review E*, **79** 031502 (2009).